FP 4A 2022

Collisions

Ramsauer effect

Electron collisions

Low energy collisions with molecules

De Broglie wave length

$$\lambda = \frac{h}{p} = \frac{h}{mv}\sqrt{1 - \frac{v^2}{c^2}}$$

$$\lambda_e(4K) \sim 540\,A \sim 54x10^{-9}\,m$$

$$\lambda_e(1eV) \sim 11.6\,A \sim 1.16x10^{-9}\,m$$

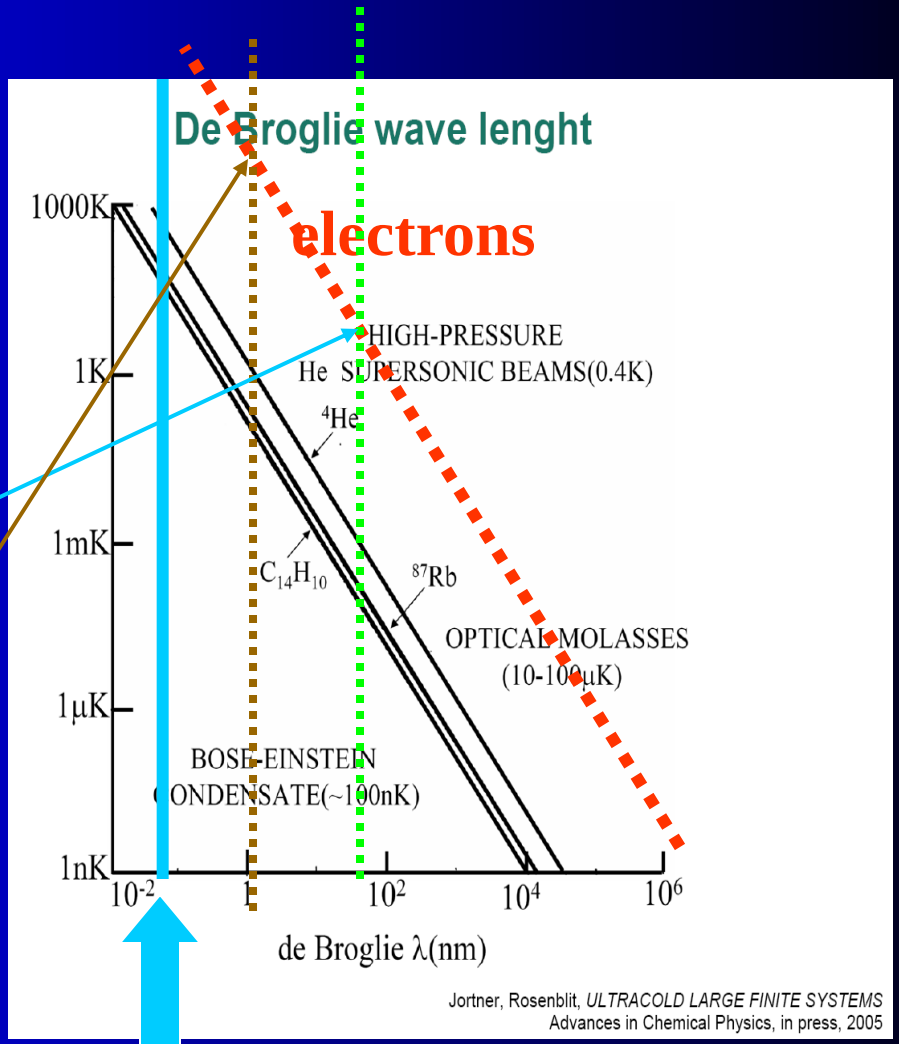

a_0

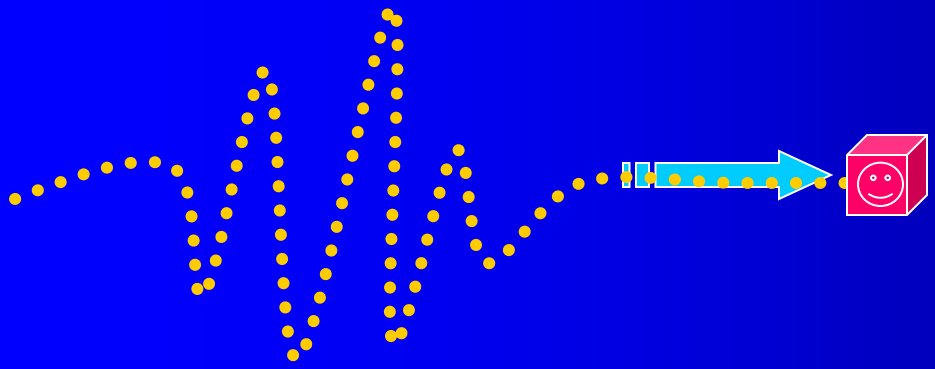

Collisions of electrons with atoms

Classical or quantum approach?

Electron:

1eV → $v=5.9\times10^{7}$cm s^{-1}

$\tau\sim a_0/v \sim 10^{-8}/ 5.9\times10^{7}=2\times10^{-16}$s

$\lambda\sim 2A = 2\times10^{-8}$cm de Broglie

Ar+:

1eV → $v=2\times10^{5}$cm s^{-1}

$\tau\sim a_0/v \sim 10^{-8}/ 2\times10^{5}\sim 6\times10^{-14}$s

$\lambda\sim 9\times10^{-11}$cm de Broglie

H_3^* + e at 10 K ????

$$\lambda_e(4K) \sim 540\,A \sim 54x10^{-9}\,m$$

Rydberg atom

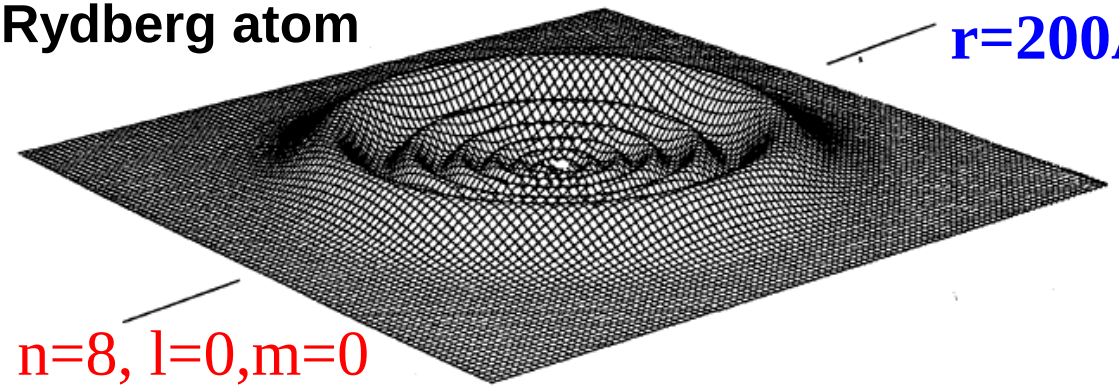

Collisions of electrons with atoms (atomic beams)

CROASED BEAM METHOD

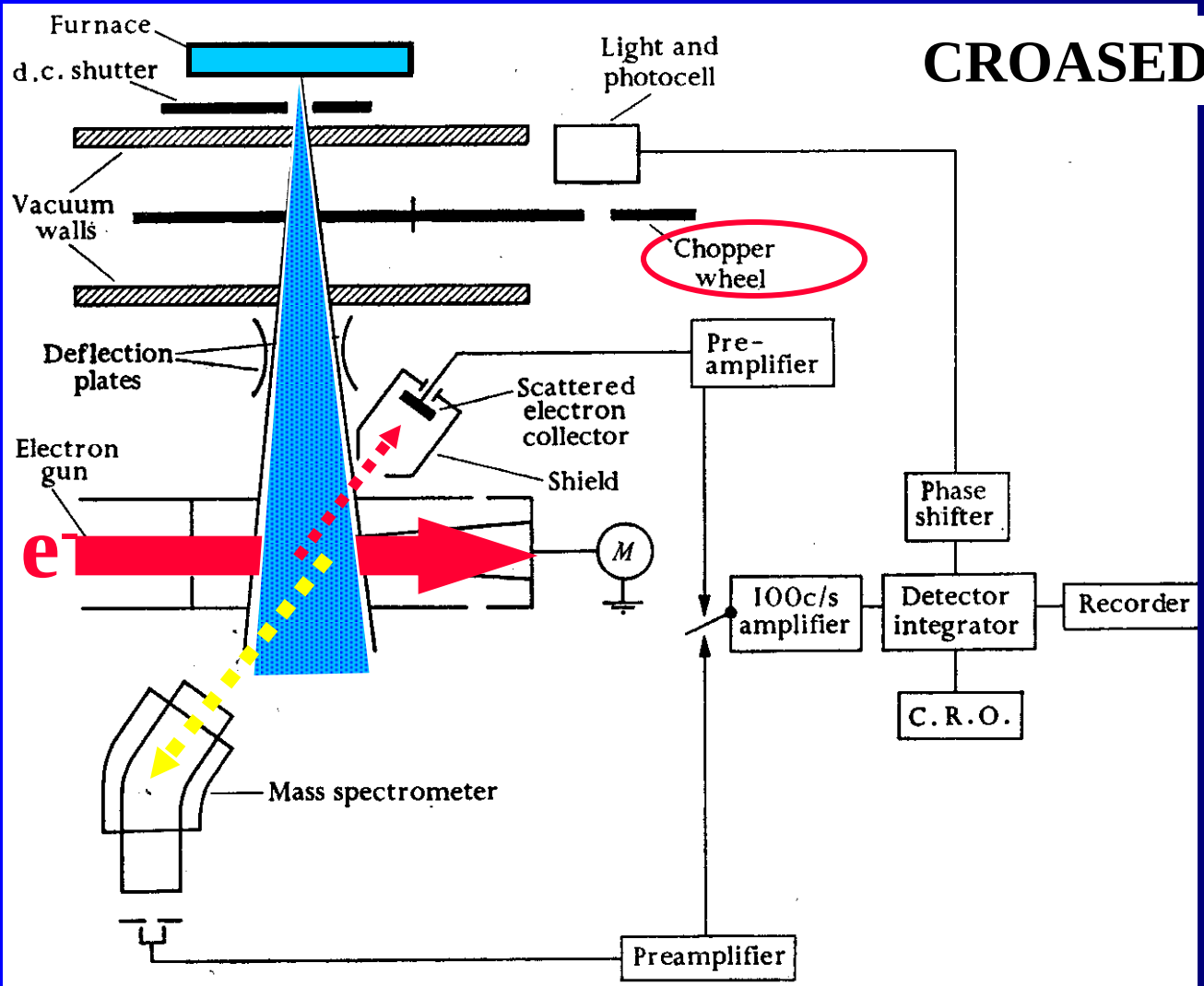

FIG. 1.2. Schematic diagram of the arrangement of apparatus used by Fite, Brackmann, and Neynaber for observation of elastic scattering of electrons by atomic hydrogen.

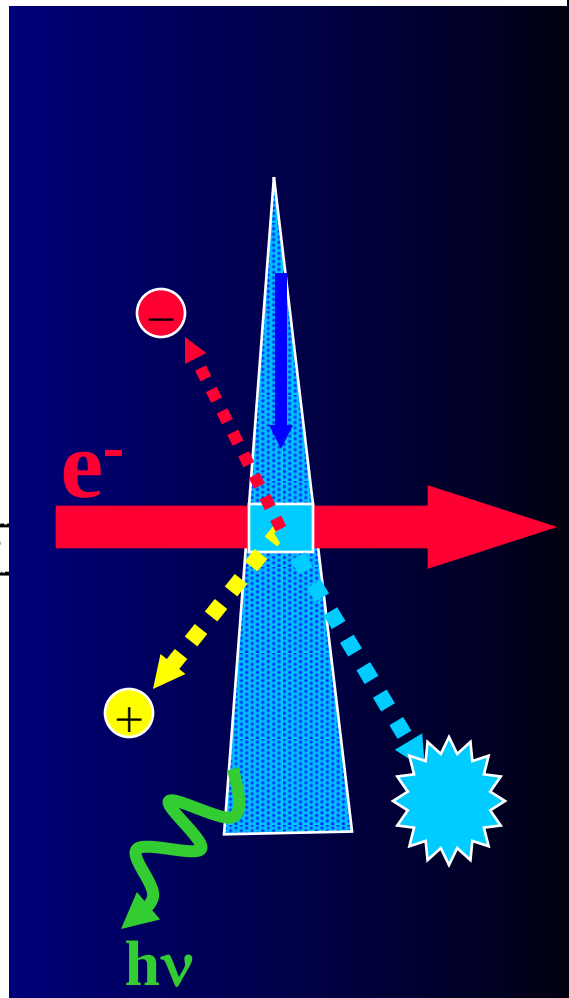

Position (angle), mass and energy sensitive detectors

Partial cross section for excitation

Collisions with e

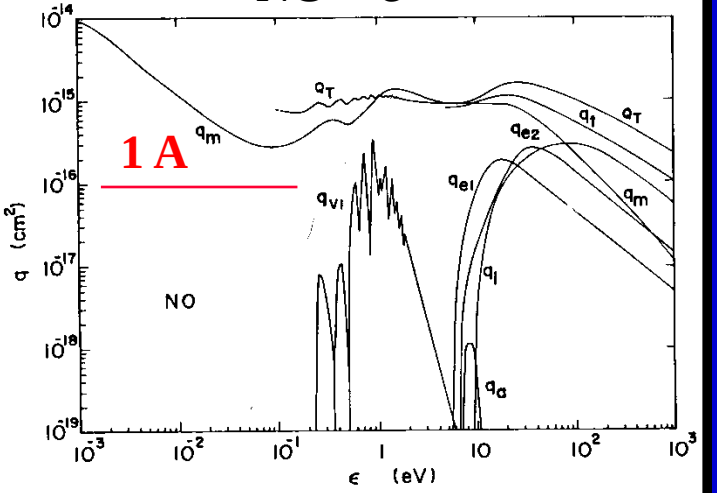

Fig. 4. Cross-section set for NO (1986).

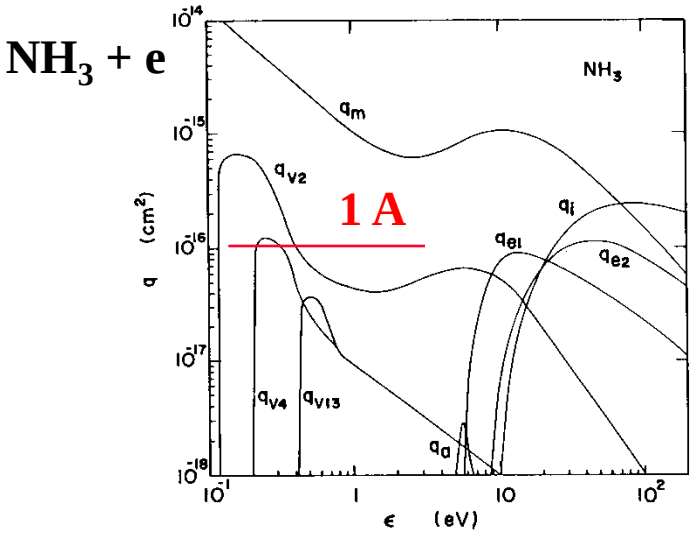

Fig. 6. Electron collision cross-section set for NH_3 (1986).

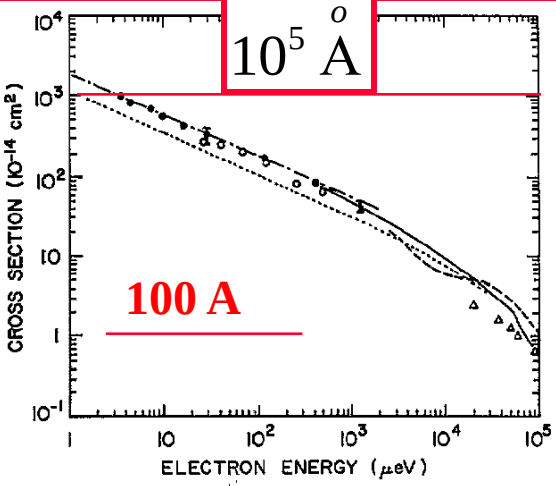

Figure 3. Cross sections for electron attachment to CCl_4. ●, $\bar{\sigma}_e$-K(np); —·—, $\sigma_c(v)$-K(np) (Frey *et al* 1994b); ○, $\bar{\sigma}_e$-K(np) (Ling *et al* 1992); ——, free electrons (Hotop 1994); – – –, free electrons (Orient *et al* 1989); △, free electrons (Christodoulides and Christophorou (1971); -----, theory (Klots 1976).

$$e^- + SF_6 \rightarrow SF_6^{-*}$$

$$e^- + CCl_4 \rightarrow CCl_4^{-*} \rightarrow CCl_3 + Cl^-$$

Total collision cross sections Na, K, Cs…

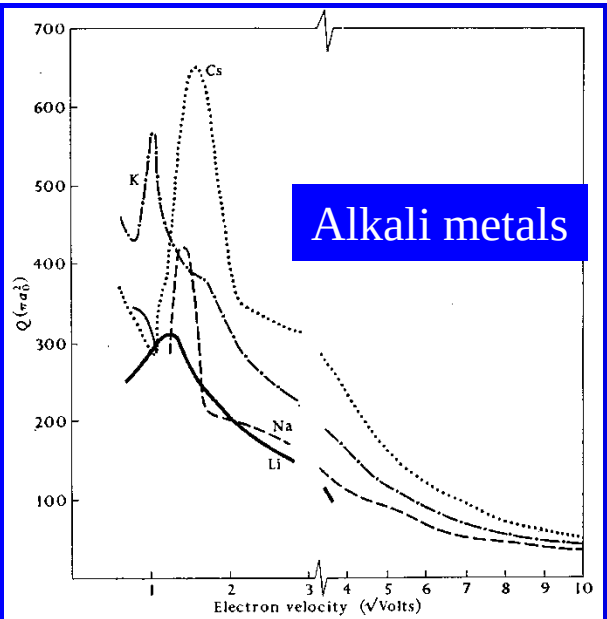

FIG. 1.16. Observed total collision cross-sections of Li, Na, K, and Cs.

Collisions with e

Alkali metals

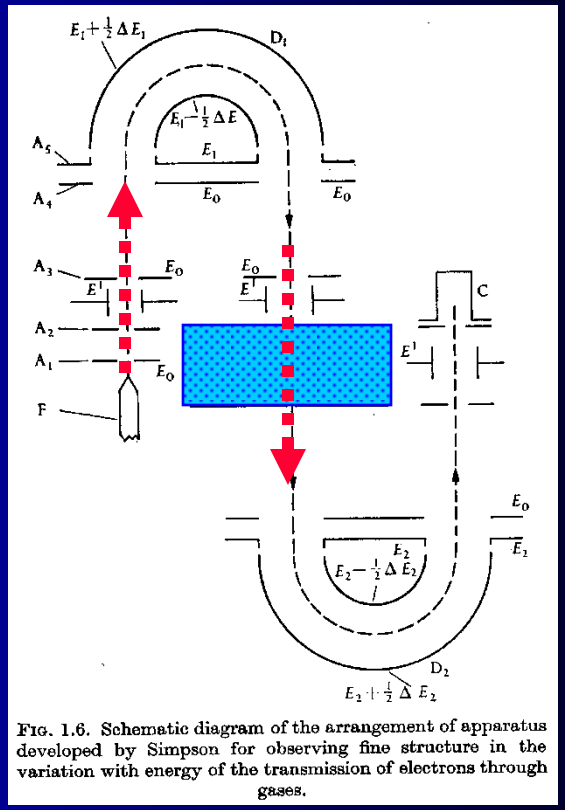

FIG. 1.6. Schematic diagram of the arrangement of apparatus developed by Simpson for observing fine structure in the variation with energy of the transmission of electrons through gases.

Cs

$e^-_{(v)}$

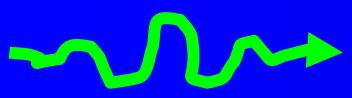

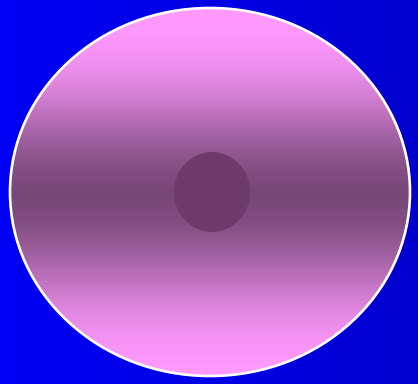

Collisions with e

Total collision and reactive cross sections comparison

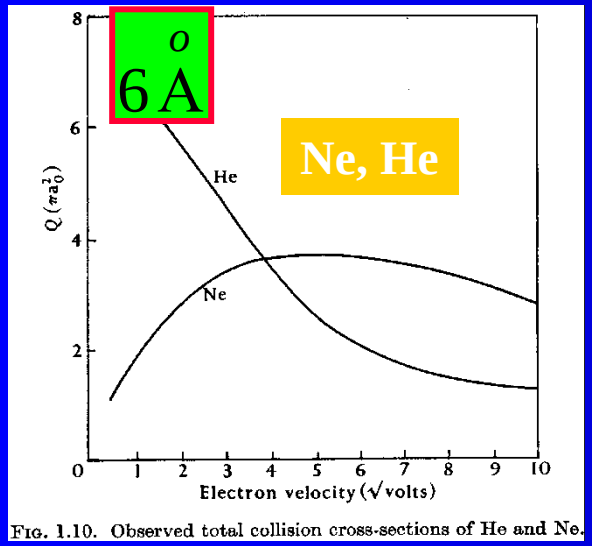

FIG. 1.10. Observed total collision cross-sections of He and Ne.

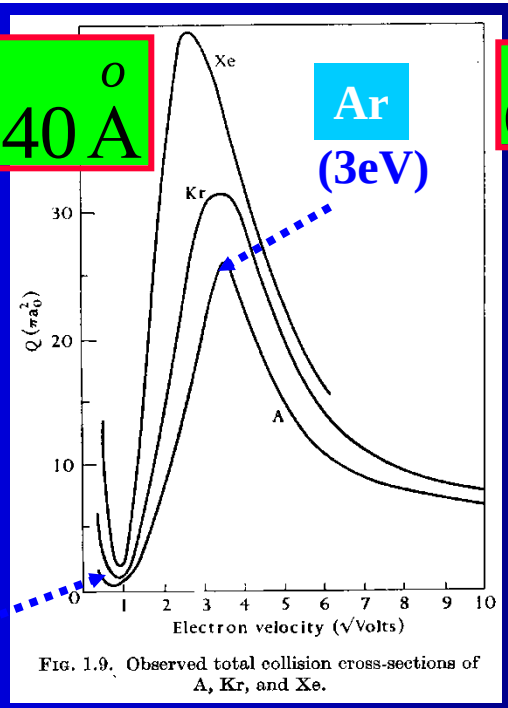

FIG. 1.9. Observed total collision cross-sections of A, Kr, and Xe.

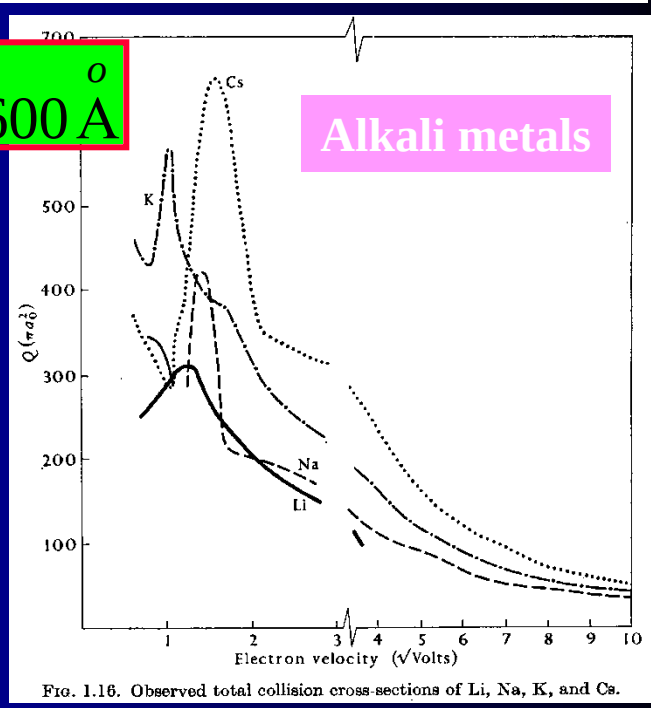

FIG. 1.16. Observed total collision cross-sections of Li, Na, K, and Cs.

(0,3eV)

σ(v)

e⁻ (v)

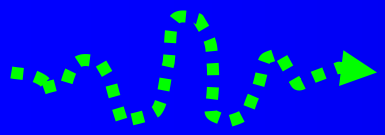

Ar

(3eV)

Ne

Ar

(0.3eV)

500A

Cs

(2eV)

100 000 Å

1μeV

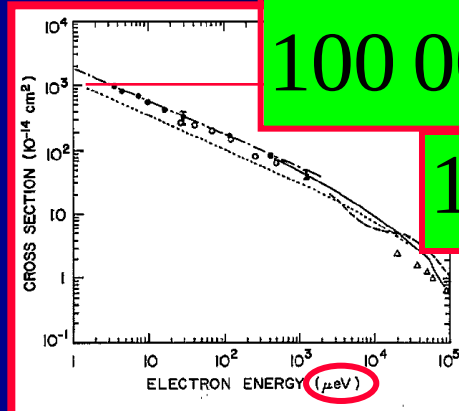

CCl_4

Figure 3. Cross sections for electron attachment to CCl_4. ●, $\bar{\sigma}_e$-K(*np*) (Frey *et al* 1994b); ○, $\bar{\sigma}_e$-K(*np*) (Ling *et al* 1992); ——, free electrons (Hotop 1994); – – –, free electrons (Orient *et al* 1989); △, free electrons (Christodoulides and Christophorou (1971); -----, theory (Klots 1976).

Collisions of electrons with atoms – Ramsauer's method

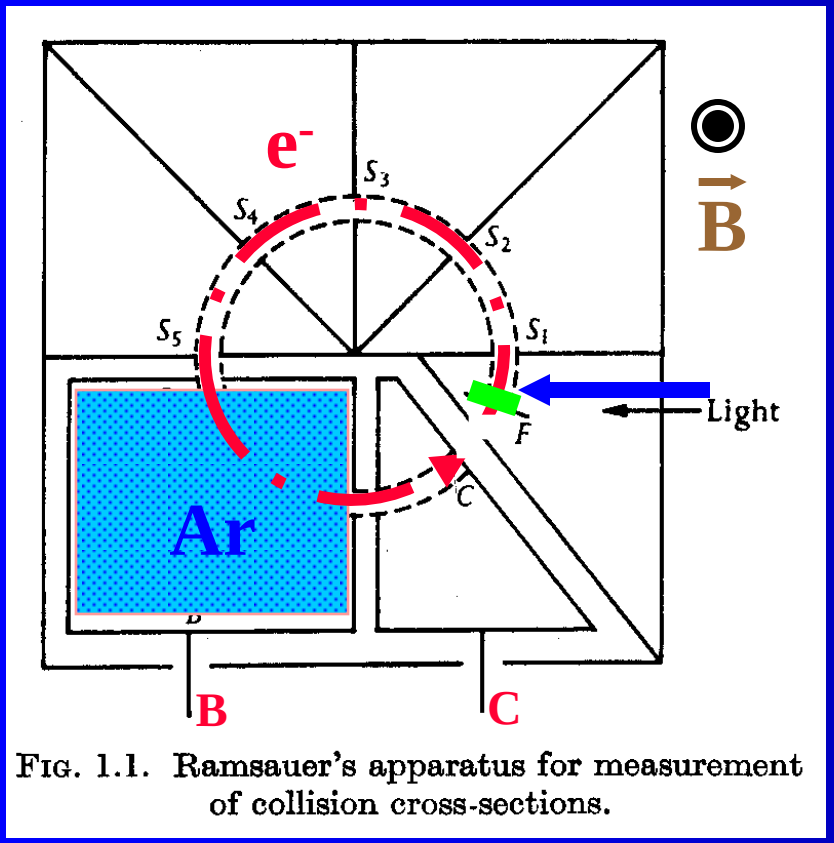

FIG. 1.1. Ramsauer's apparatus for measurement of collision cross-sections.

Lenard 1903
Akesson 1916
Ramsauer 1921

ATENUATION METHOD

$$\delta I = -N\sigma I_p \, \delta x$$

$$I_P = I_0 \exp(-\sigma N x)$$

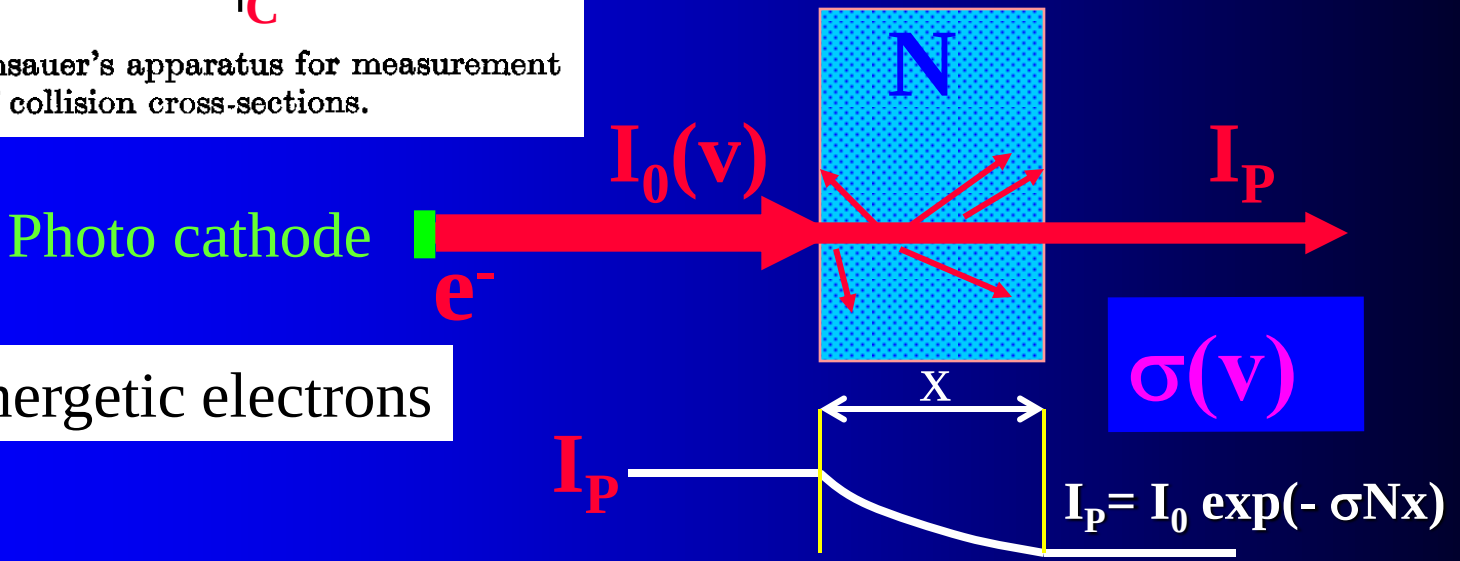

Mono energetic electrons

Collisions of electrons with atoms – Ramsauer's method

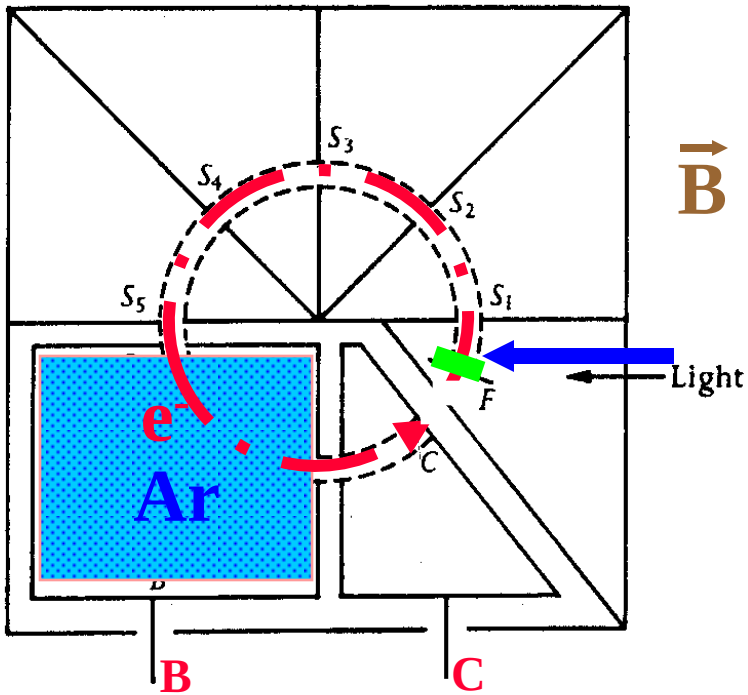

FIG. 1.1. Ramsauer's apparatus for measurement of collision cross-sections.

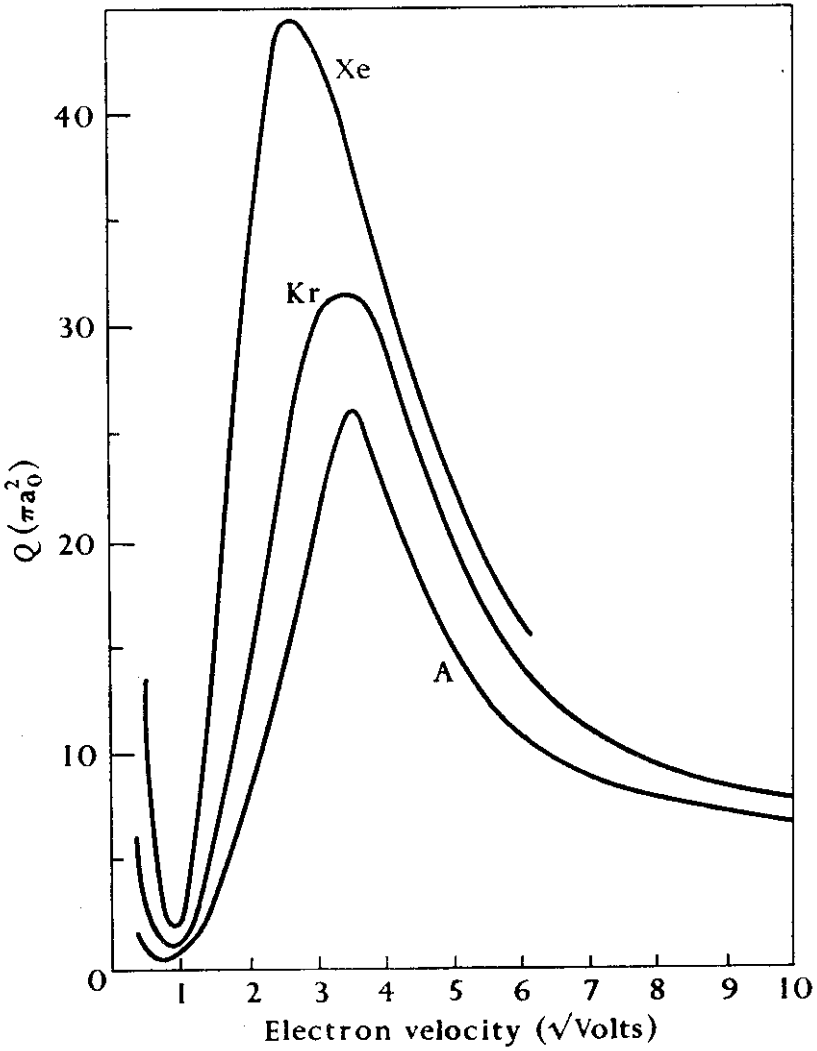

FIG. 1.9. Observed total collision cross-sections of A, Kr, and Xe.

Lenard 1903
Akesson 1916
Ramsauer 1921

Total collision cross section – e/atoms

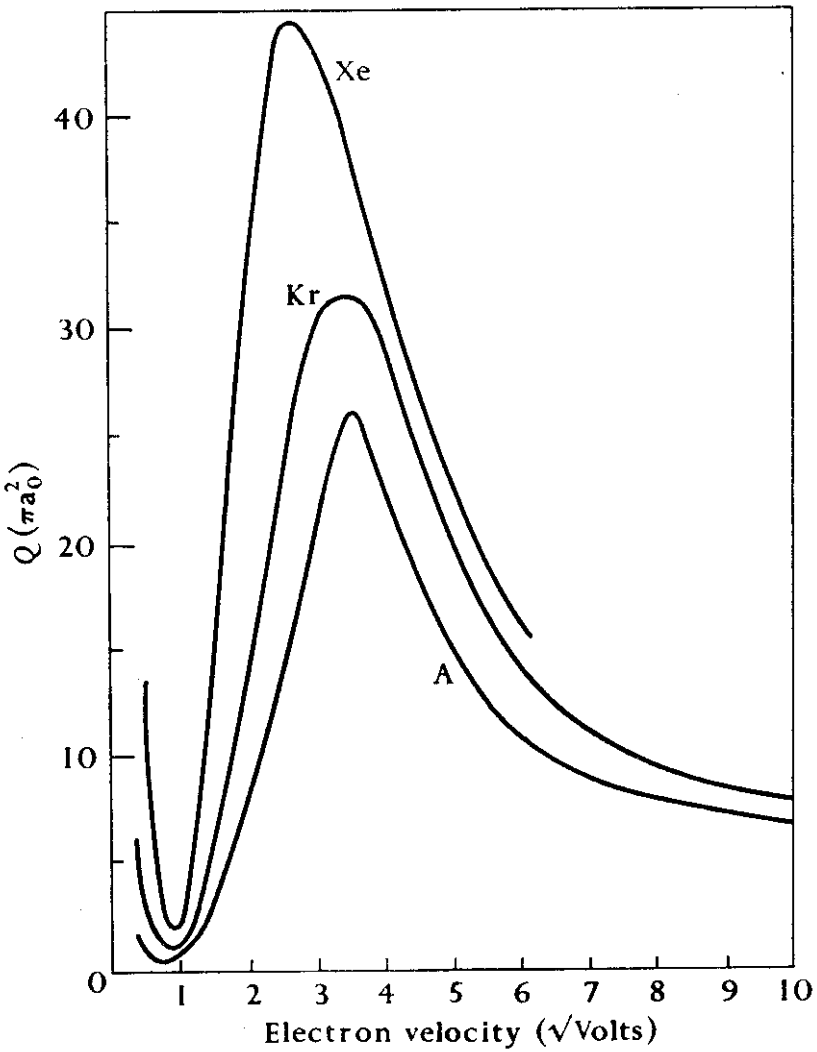

FIG. 1.9. Observed total collision cross-sections of A, Kr, and Xe.

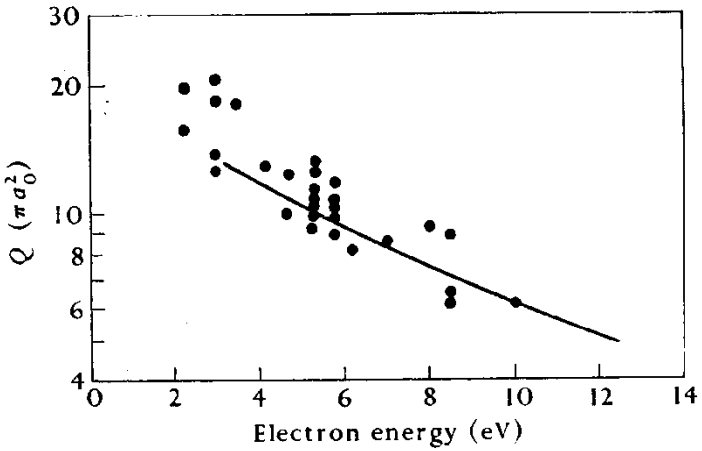

FIG. 1.11. Total collision cross-sections of atomic hydrogen. ● observed by Brackmann, Fite, and Neynaber; —— observed by Neynaber, Marino, Rothe, and Trujillo.

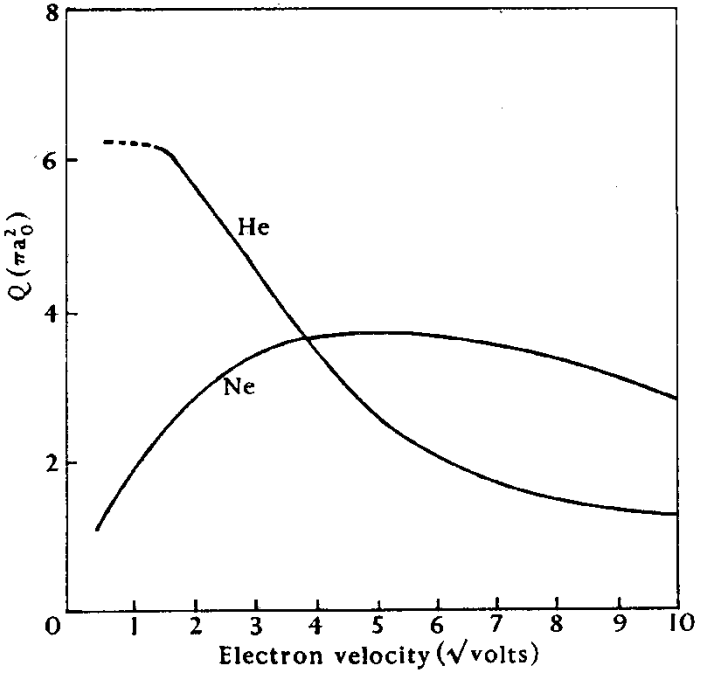

FIG. 1.10. Observed total collision cross-sections of He and Ne.

$a_0 = 0.53 \times 10^{-8}$ cm ~ 0.5A

Radius of the first Bohr orbit of H atom

Details of Ramsauer effect

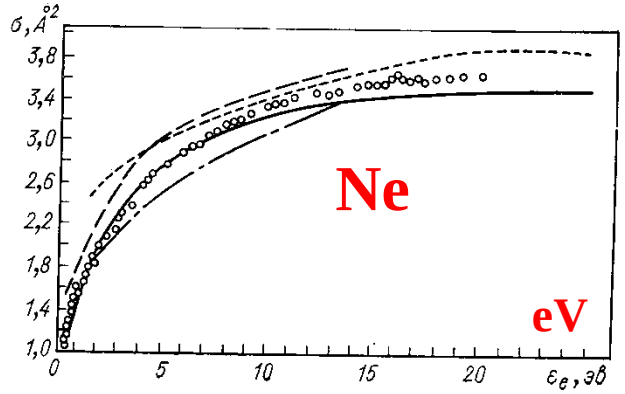

Рис. 5.8. Полное сечение рассеяния электрона на атоме неона.

Эксперимент (метод Рамзауэра): ○ — [101]; ——— — [29]; ····· —[92]; — · — — [95]. Теория: — — — [109].

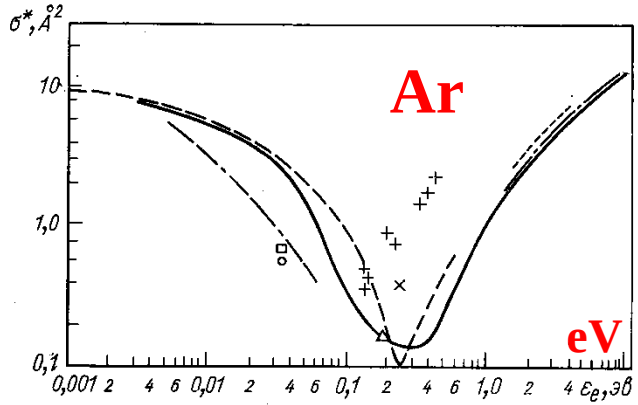

Рис. 5.9. Диффузионное сечение столкновения электрона с атомом аргона.

Эксперимент (подвижность электронов при малых полях и температурах): ····· — [21]; ——— — [47]; × — [60]; ○ — [91]; □ — [112]; △ — [44]; — · — — [16]; — — · — — — [108]; + — [43]. Теория: — — — [87].

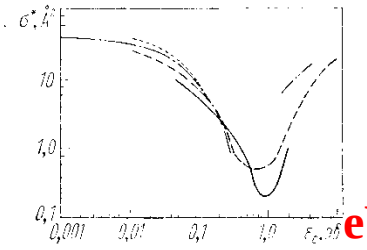

Kr

Рис. 5.12. Диффузионное сечение столкновения электрона с атомом криптона.

Эксперимент (подвижность электронов при малых полях и температурах): ····· — [34]; — ·· — — [21]; — — — — [47]; ——— — [63]. Теория: — · — — [87].

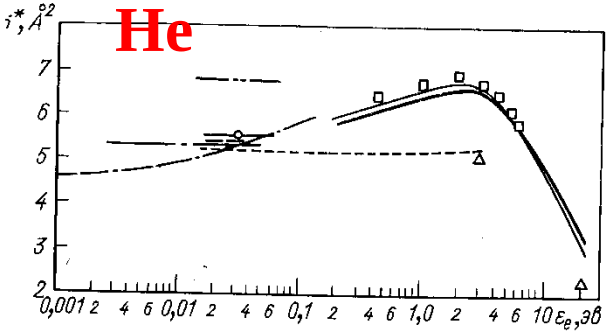

Рис. 5.3. Диффузионное сечение столкновения электрона с атомом гелия.

Эксперимент (подвижность электронов при малых полях и температурах): □ — [39]; △ — [73]; — · — — [88]; — — — — [91]; ····· — [58]; — ····· — — [13]; —○— — [62]. Теория: ——— — [75]; ——— — [32]; — · — · — расчет по формуле (5.37).

Frequencies of elastic collisions

$\delta I = -NQI_p \delta x$

$I_P = I_0 \exp(-QNx)$

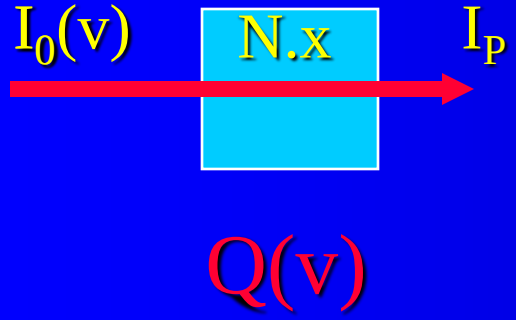

$a_0 = 0.53 \times 10^{-8}$cm~0.5A

Radius of the first Bohr orbit of H atom

$\nu \sim n v \sigma$

Collision Frequencies

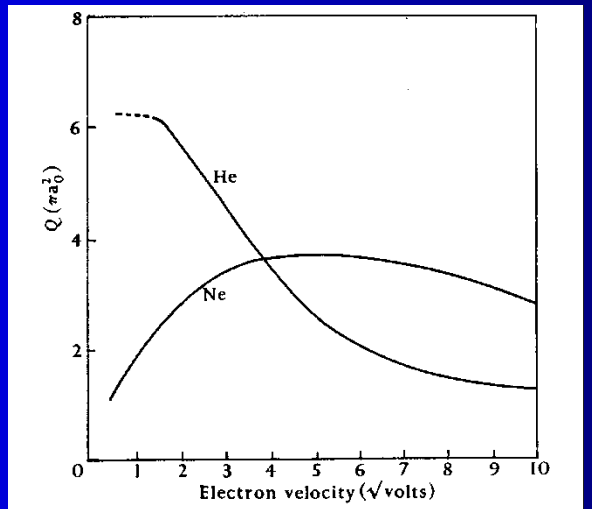

FIG. 1.10. Observed total collision cross-sections of He and Ne.

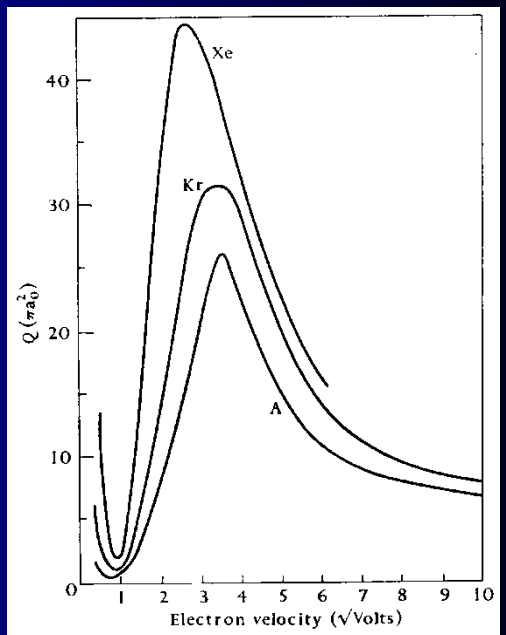

FIG. 1.9. Observed total collision cross-sections of A, Kr, and Xe.

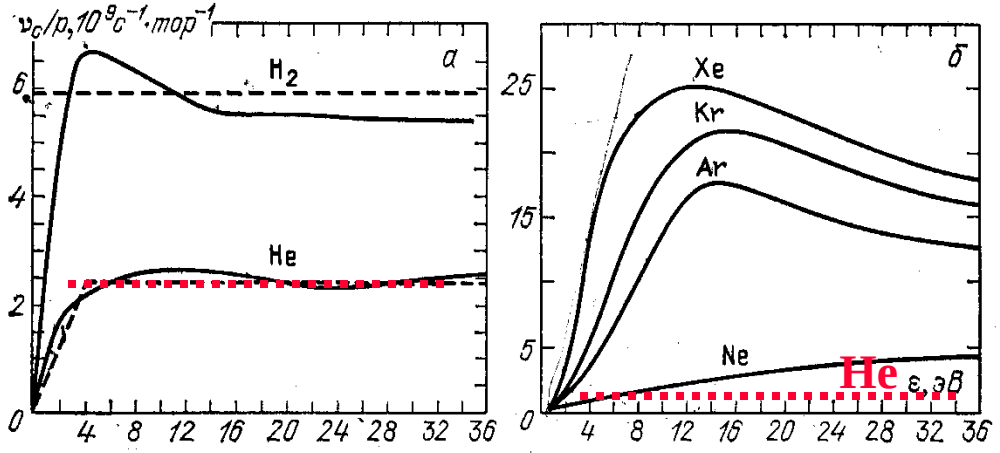

Рис. 2.5. Частоты упругих столкновений электронов, p=1 тор: *а* — в H_2 и He; *б* — в инертных газах; штриховые линии — удобная аппроксимация при расчетах [24]

Total collision and reactive cross sections comparison

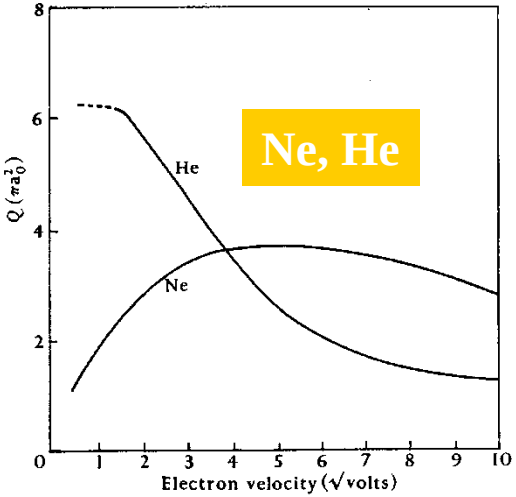

FIG. 1.10. Observed total collision cross-sections of He and Ne.

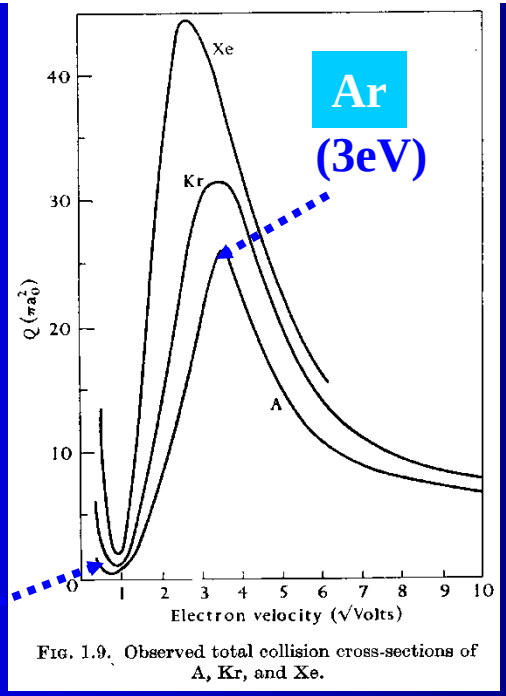

FIG. 1.9. Observed total collision cross-sections of A, Kr, and Xe.

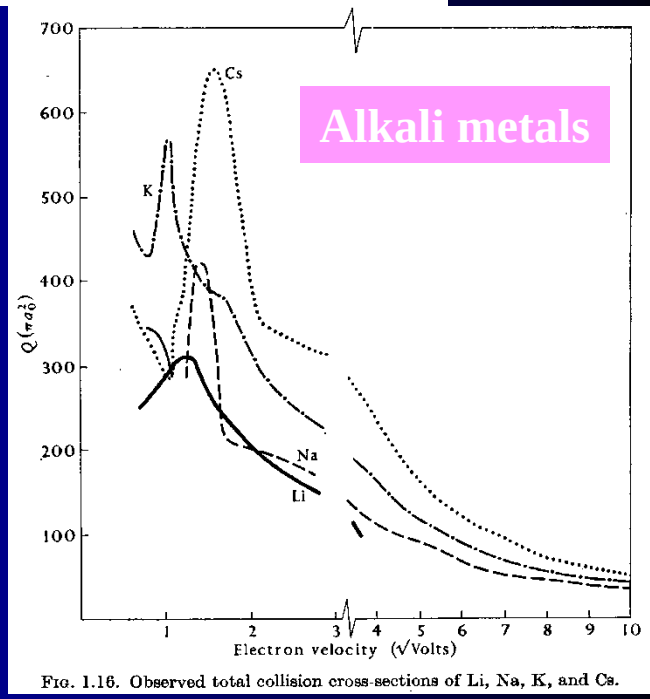

FIG. 1.16. Observed total collision cross-sections of Li, Na, K, and Cs.

(0,3eV)

σ(v)

e⁻ (v)

Ar
(3eV)

Ne

Ar
(0.3eV)

500A

Cs

(2eV)

100 000 Å

1μeV

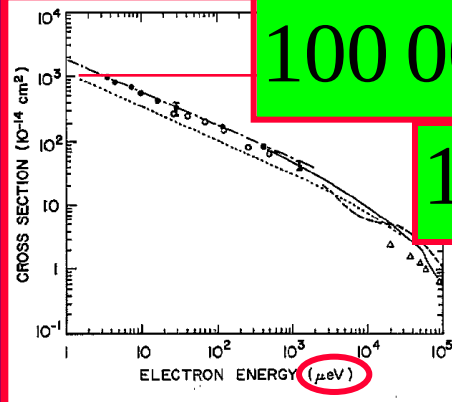

CCl_4

Figure 3. Cross sections for electron attachment to CCl_4. ●, $\bar{\sigma}_e$-K(*np*) (Frey *et al* 1994b); ○, $\bar{\sigma}_e$-K(*np*) (Ling *et al* 1992); ——, free electrons (Hotop 1994); – – –, free electrons (Orient *et al* 1989); △, free electrons (Christodoulides and Christophorou (1971); -----, theory (Klots 1976).

Kvantová mechanika
Jednorozměrný rozptyl

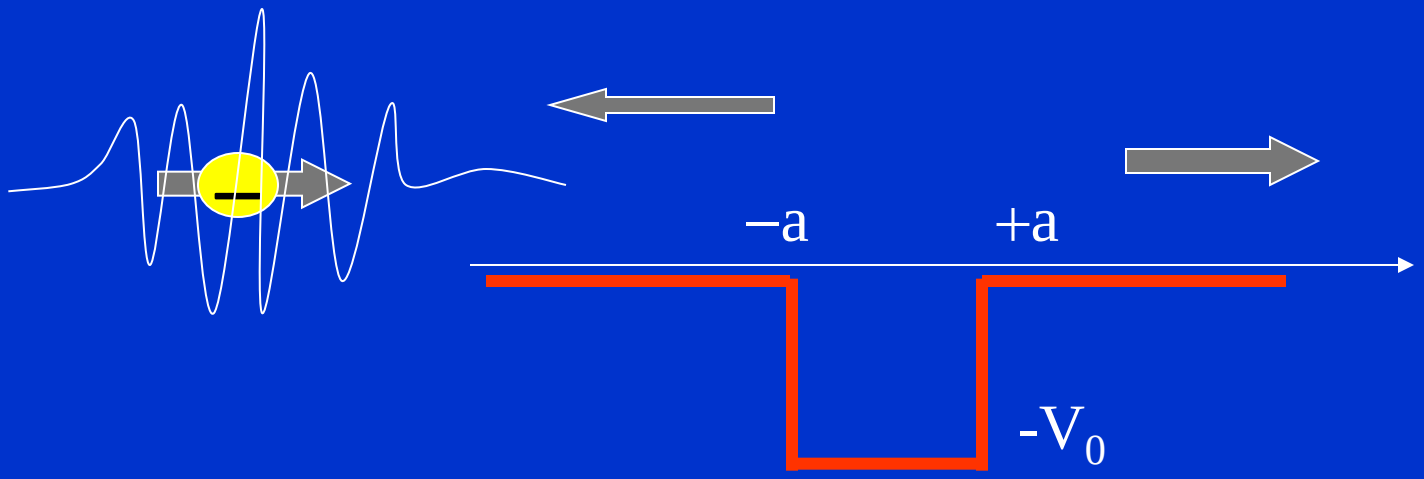

Kvantová mechanika I
J. Klíma B. Velický
MFF 1992

Jednorozměrný rozptyl

Vlnová funkce má tvar superposice Brogoliových vln

$k = \sqrt{2mE/h^2}$

$\psi_k(x,t) = (Ae^{ikx} + Be^{-ikx})e^{iE_k t/h} \quad x \le -a$

$k = \sqrt{2mE/h^2}$

$\psi_k(x,t) = (Fe^{ikx} + Ge^{-ikx})e^{iE_k t/h} \quad x > a$

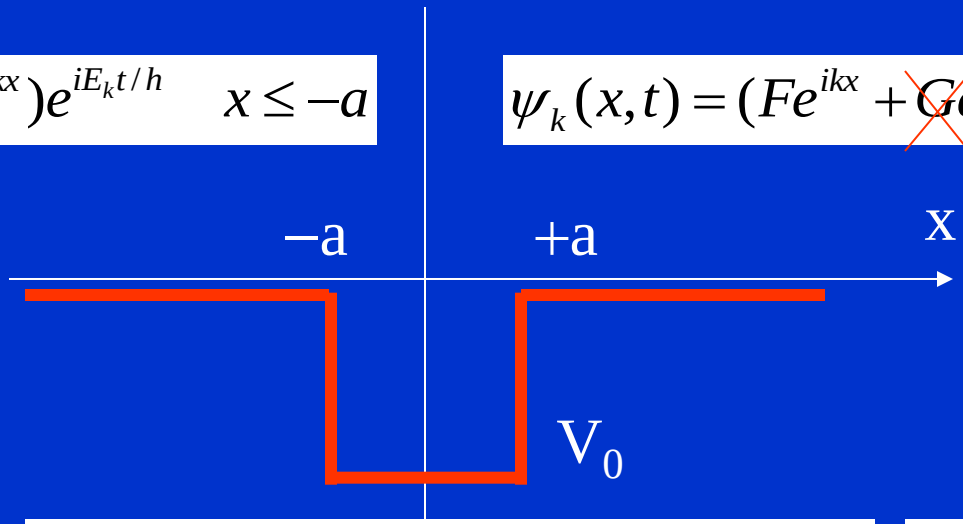

$\psi_k(x,t) = (Ce^{ik'x} + De^{-ik'x})e^{iE_k t/h} \quad |x| \le a$

$k' = \sqrt{2m(E+V_0)/h^2}$

a) dopadající částice ➔A

b) odražená částice ➔B

c) procházející částice ➔F≠0, G=0

Jednorozměrný rozptyl

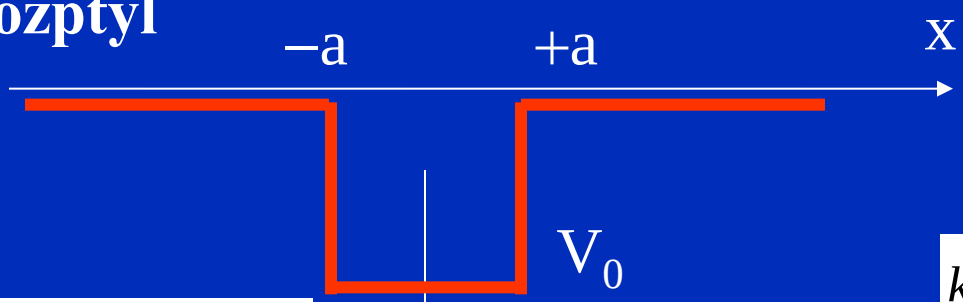

$$k = \sqrt{2mE/h^2}$$

$$k' = \sqrt{2m(E+V_0)/h^2}$$

$$\psi_k(x,t) = (Ae^{ikx} + Be^{-ikx})e^{iE_k t/h} \qquad x \le -a$$

$$\psi_k(x,t) = (Ce^{ik'x} + De^{-ik'x})e^{iE_k t/h} \qquad |x| \le a$$

$$\psi_k(x,t) = (Fe^{ikx})e^{iE_k t/h} \qquad x > a$$

Parametry jsou E, V_0 , a

Hladkost řešení v bodech ±a
Urči konstanty B, C, D, G,
Hodnota A je vstupní parametr

Tok dopadajících částic $j_{in} = \frac{hk}{m}|A|^2$

Tok odražených částic $j_{rf} = \frac{hk}{m}|B|^2$

Tok prošlých částic $j_{tr} = \frac{hk}{m}|F|^2$

Jednorozměrný rozptyl

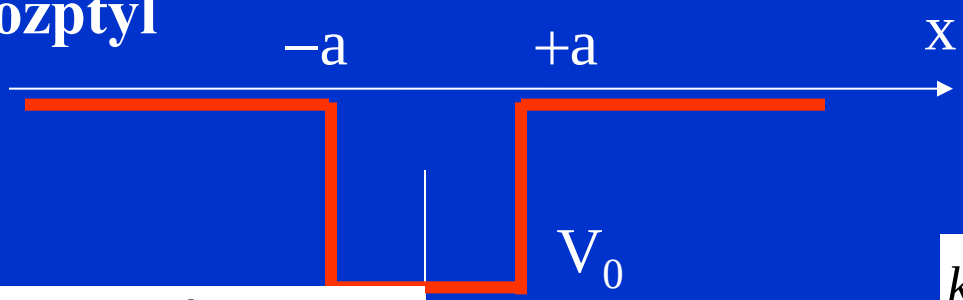

$$k = \sqrt{2mE/h^2}$$

$$k' = \sqrt{2m(E+V_0)/h^2}$$

$$\psi_k(x,t) = (Ae^{ikx} + Be^{-ikx})e^{iE_k t/h} \qquad x \le -a$$

$$\psi_k(x,t) = (Ce^{ik'x} + De^{-ik'x})e^{iE_k t/h} \qquad |x| \le a$$

$$\psi_k(x,t) = (Fe^{ikx})e^{iE_k t/h} \qquad x > a$$

Parametry jsou E, V_0 , a

Hladkost řešení v bodech ±a
Urči konstanty B, C, D, G,
Hodnota A je vstupní parametr

Tok dopadajících částic $j_{in} = \frac{hk}{m}|A|^2$

Tok odražených částic $j_{rf} = \frac{hk}{m}|B|^2$

Tok prošlých částic $j_{tr} = \frac{hk}{m}|F|^2$

$$C = \frac{F}{2}(1 + k/k')e^{i(k-k')a}$$

$$D = \frac{F}{2}(1 - k/k')e^{i(k+k')a}$$

Jednorozměrný rozptyl

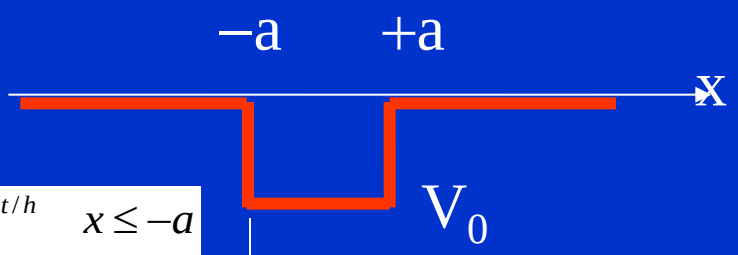

$$k = \sqrt{2mE/h^2}$$

$$k' = \sqrt{2m(E+V_0)/h^2}$$

$$\psi_k(x,t) = (Ae^{ikx} + Be^{-ikx})e^{iE_k t/h} \qquad x \le -a$$

$$\psi_k(x,t) = (Ce^{ik'x} + De^{-ik'x})e^{iE_k t/h} \qquad |x| \le a$$

$$\psi_k(x,t) = (Fe^{ikx})e^{iE_k t/h} \qquad x > a$$

Parametry jsou E, V_0 , a

$$j_{in} = \frac{hk}{m}|A|^2$$

$$j_{rf} = \frac{hk}{m}|B|^2$$

$$j_{tr} = \frac{hk}{m}|F|^2$$

Hladkost řešení v bodech ±a
Urči konstanty B, C, D, F,
Hodnota A je vstupní parametr

$$\varepsilon = \frac{k'}{k} + \frac{k}{k'}$$

$$A = e^{2ika}(\cos(2k'a) - i(\varepsilon/2)\sin(2k'a))F$$

Koeficient průchodu T, koeficient odrazu R

$$\frac{1}{T} = \left|\frac{A}{F}\right|^2 = 1 + \frac{V_0^2}{4E(E+V)}\sin^2(2k'a)$$

Jednorozměrný rozptyl

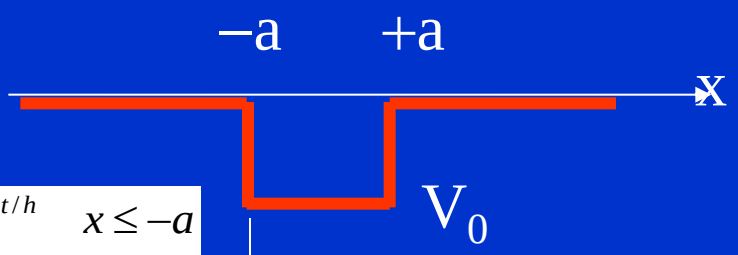

$$k = \sqrt{2mE/h^2}$$

$$k' = \sqrt{2m(E+V_0)/h^2}$$

$$\psi_k(x,t) = (Ae^{ikx} + Be^{-ikx})e^{iE_k t/h} \qquad x \le -a$$

$$\psi_k(x,t) = (Ce^{ik'x} + De^{-ik'x})e^{iE_k t/h} \qquad |x| \le a$$

$$\psi_k(x,t) = (Fe^{ikx})e^{iE_k t/h} \qquad x > a$$

Parametry jsou E, V_0 , a

$$j_{in} = \frac{hk}{m}|A|^2$$

$$j_{rf} = \frac{hk}{m}|B|^2$$

$$j_{tr} = \frac{hk}{m}|F|^2$$

Koeficient průchodu T, koeficient odrazu R

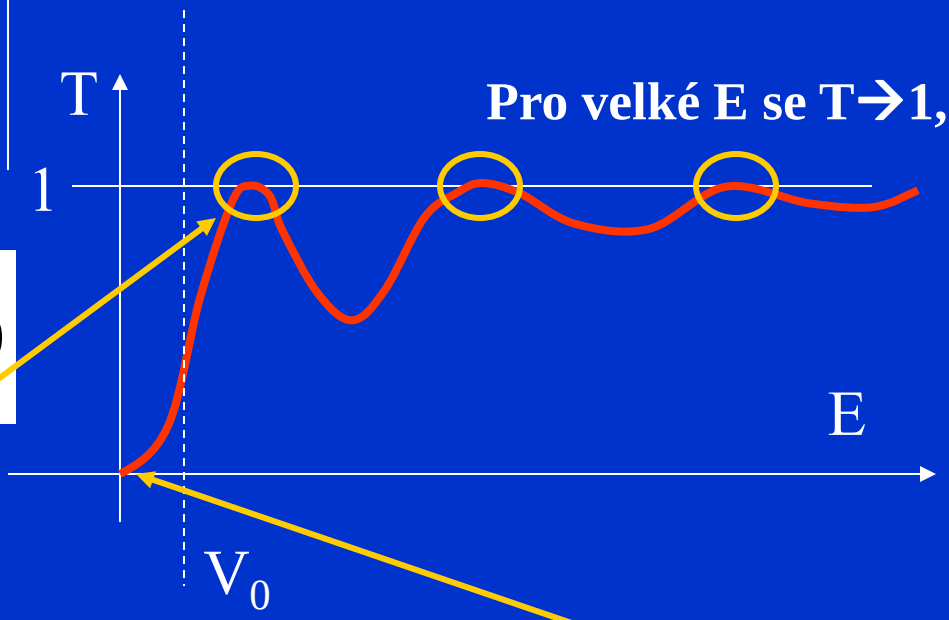

Pro velké E se T→1,

$$\frac{1}{T} = \left|\frac{A}{F}\right|^2 = 1 + \frac{V_0^2}{4E(E+V_0)}\sin^2(2k'a)$$

T=1 pro

$$2k_n'a = n\pi$$

$$\lim_{E\to 0}\frac{1}{T} \sim 1 + \frac{V_0^2}{4EV_0}\sin^2(2k'a) \sim 1 + \frac{V_0}{4E}\sin^2(2\sqrt{2mV_0/h^2}\,a) \sim 1 + \frac{V_0}{4E}const \sim \infty$$

$$\lim_{E\to 0} T \sim 0$$

Efekt Ramsauera - Kr

Parametry jsou E, V_0 , a

$$\frac{1}{T} = \left|\frac{A}{F}\right|^2 = 1 + \frac{V_0^2}{4E(E+V_0)}\sin^2(2k'a)$$

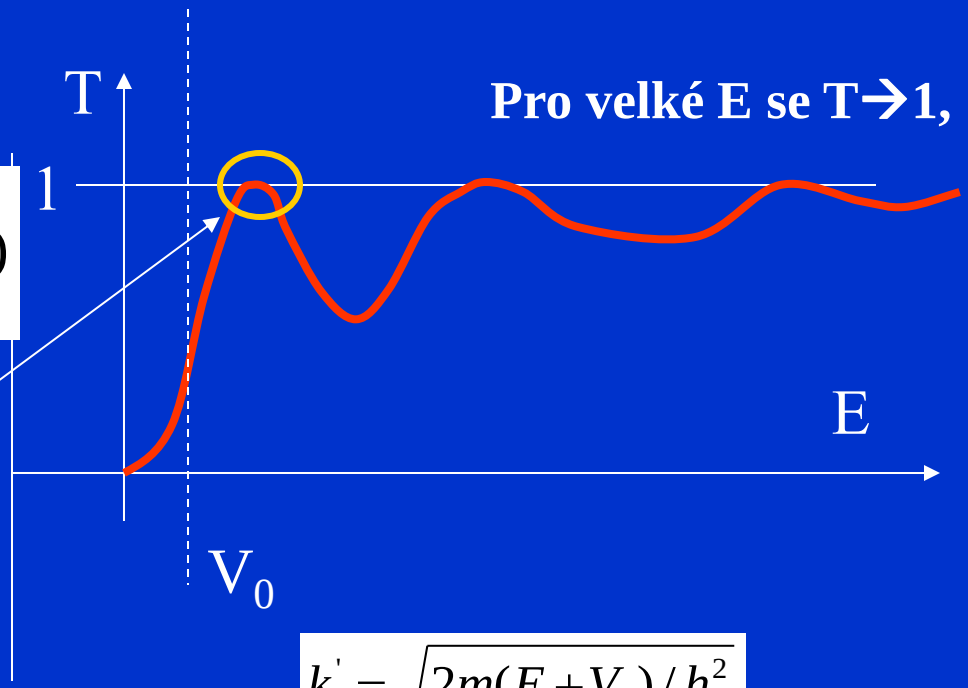

Pro velké E se T→1,

T=1 pro $2k_n'a = n\pi$

$$k' = \sqrt{2m(E+V_0)/h^2}$$

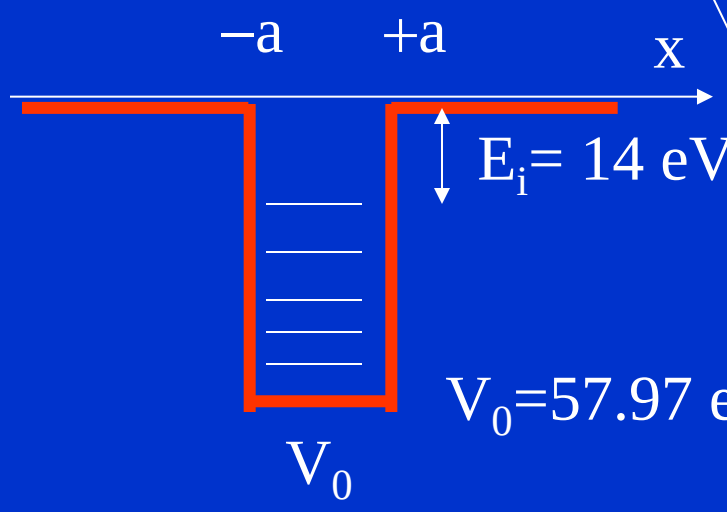

Kr; a=2Å

E_i= 14 eV ➔ V_0=57.97 eV

E=0.013 V_0=0.75 eV

Jednorozměrný rozptyl

Parametry jsou E, V_0 , a

T+R=1

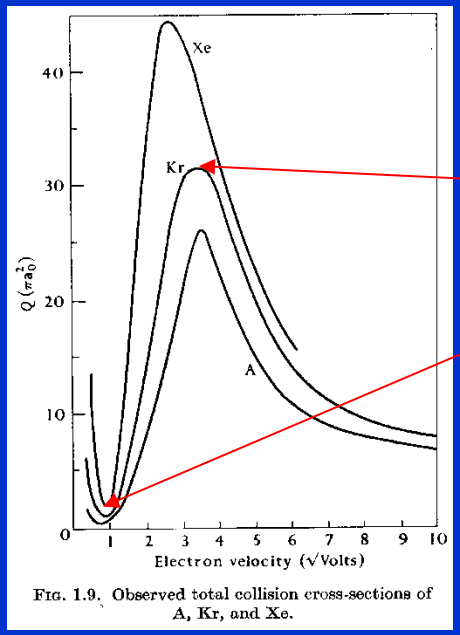

FIG. 1.9. Observed total collision cross-sections of A, Kr, and Xe.

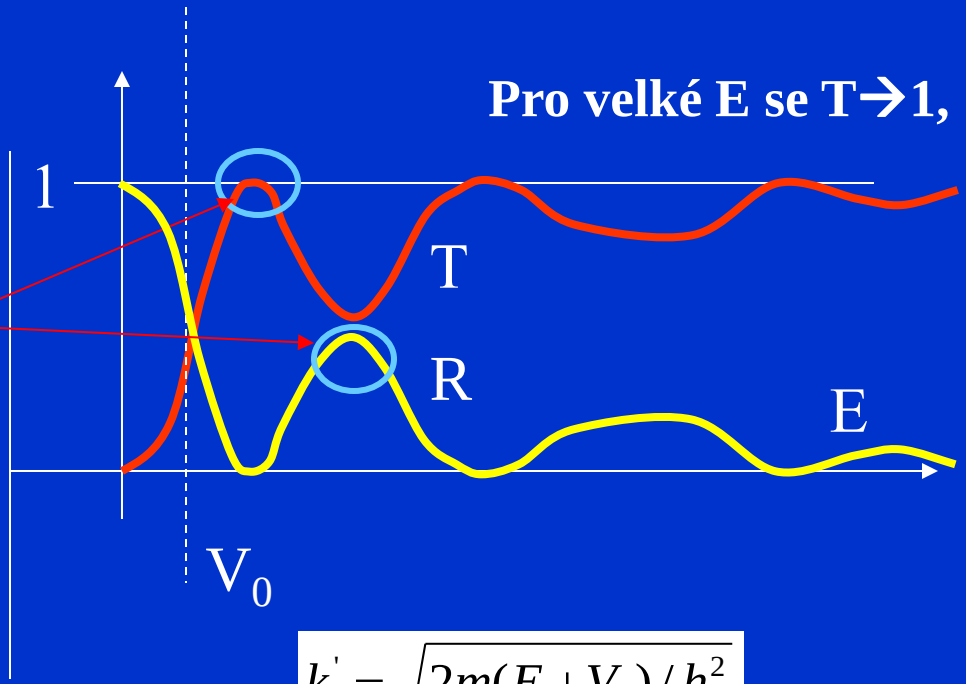

Pro velké E se T→1,

$$2k_n' a = n\pi$$

$$k' = \sqrt{2m(E+V_0)/h^2}$$

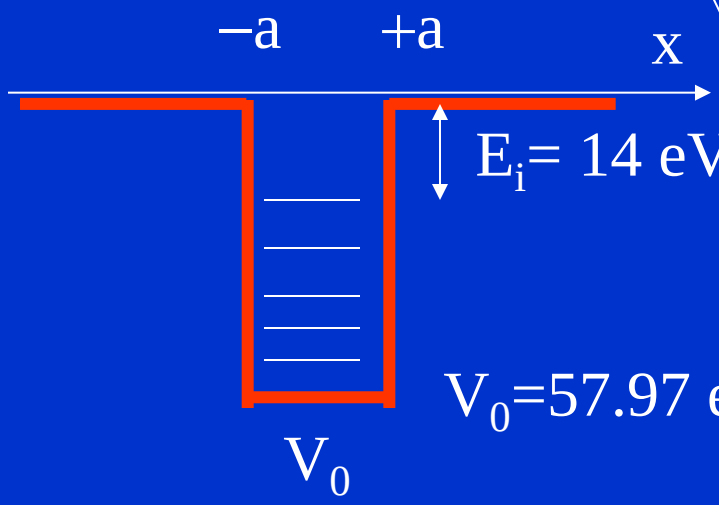

Kr; a=2Å

E_i= 14 eV ➔ V_0=57.97 eV

E=0.013 V_0=0.75 eV

Frequencies of elastic collisions

$\delta I = -NQI_p \delta x$

$I_P = I_0 \exp(-QNx)$

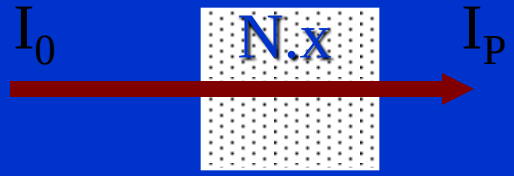

Q(v)

Collision Frequencies

$\nu \sim n v \sigma$

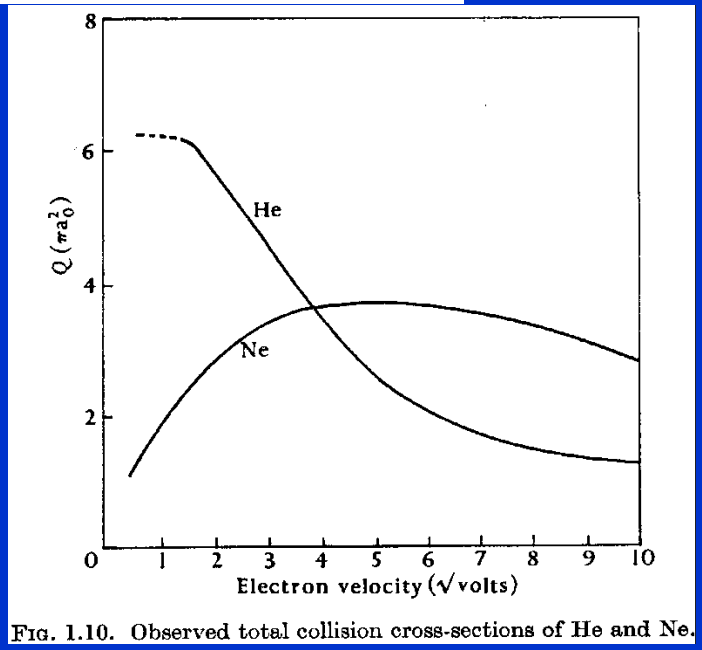

Fig. 1.10. Observed total collision cross-sections of He and Ne.

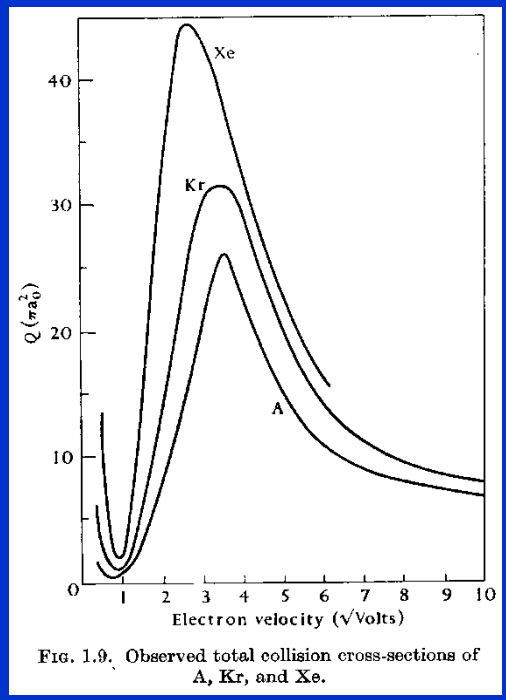

Fig. 1.9. Observed total collision cross-sections of A, Kr, and Xe.

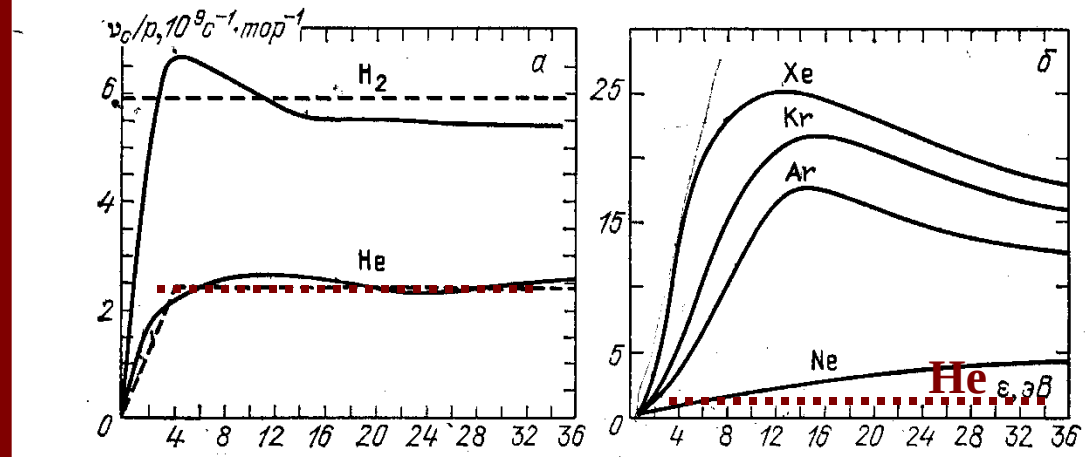

Рис. 2.5. Частоты упругих столкновений электронов, p=1 тор: *а* — в H_2 и He; *б* — в инертных газах; штриховые линии — удобная аппроксимация при расчетах [24]

$a_0 = 0.53 \times 10^{-8}$cm~0.5A

Radius of the first Bohr orbit of H atom

Koniec rosprávky 27 10 2022

Very low collision energies

1995

TOPICAL REVIEW

Electron–molecule collisions at very low electron energies

F B Dunning

Department of Physics and the Rice Quantum Institute, Rice University, PO Box 1892, Houston, TX 77251, USA

J. Phys. B: At. Mol. Opt. Phys. 28 (1995) 1645–1672. Printed in the UK

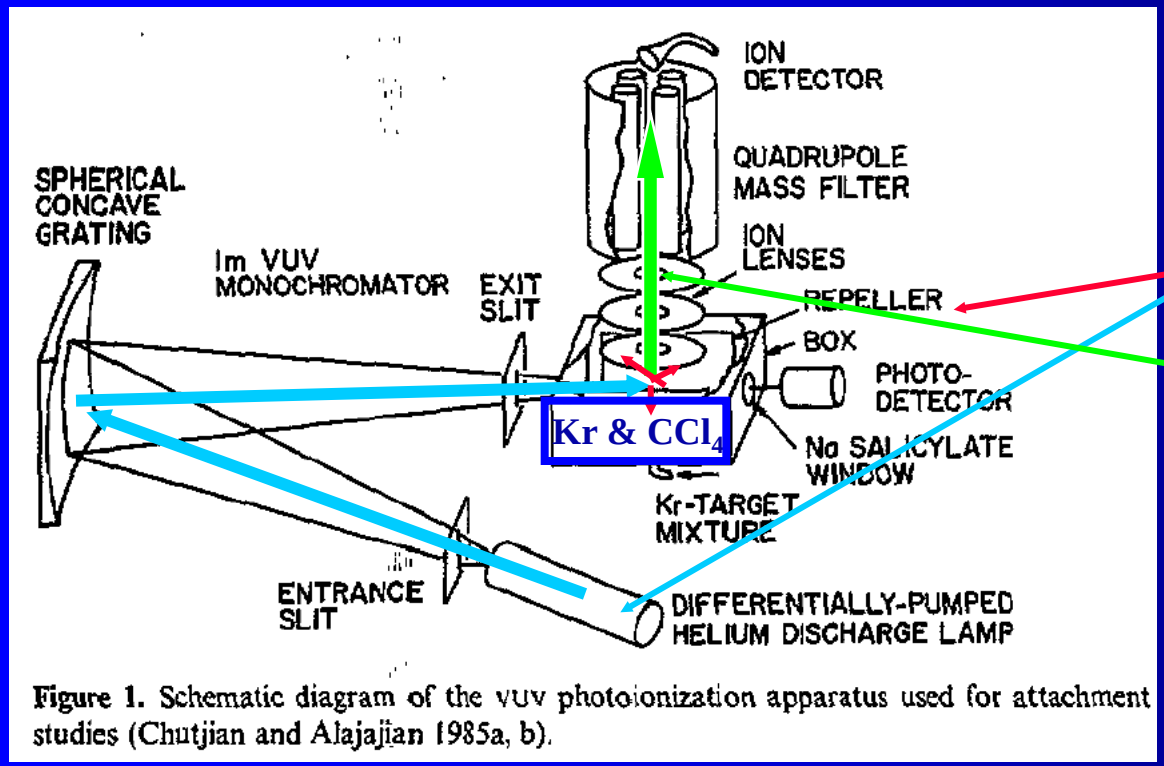

Figure 1. Schematic diagram of the VUV photoionization apparatus used for attachment studies (Chutjian and Alajajian 1985a, b).

$$Kr(^1S_0) + \hbar\omega \rightarrow Kr^+(^2P_{1/2}) + e^-(\varepsilon)$$

$$e^- + CCl_4 \rightarrow CCl_4^{-*} \rightarrow CCl_3 + Cl^-$$

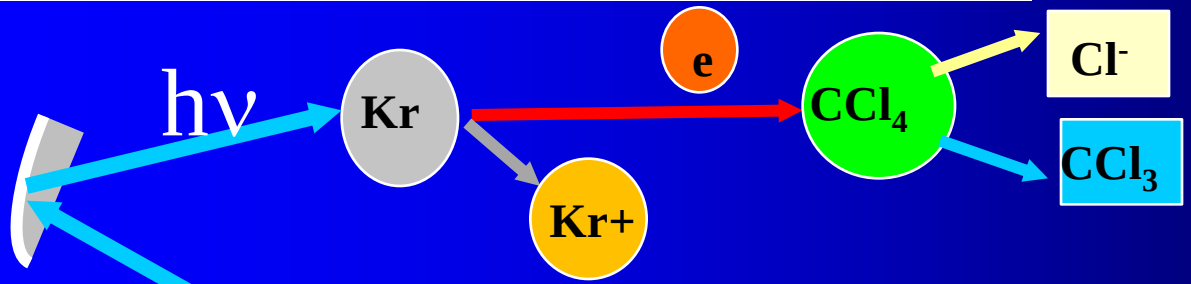

Very low collision energies

TOPICAL REVIEW

Electron–molecule collisions at very low electron energies

F B Dunning

Department of Physics and the Rice Quantum Institute, Rice University, PO Box 1892, Houston, TX 77251, USA

J. Phys. B: At. Mol. Opt. Phys. 28 (1995) 1645–1672. Printed in the UK

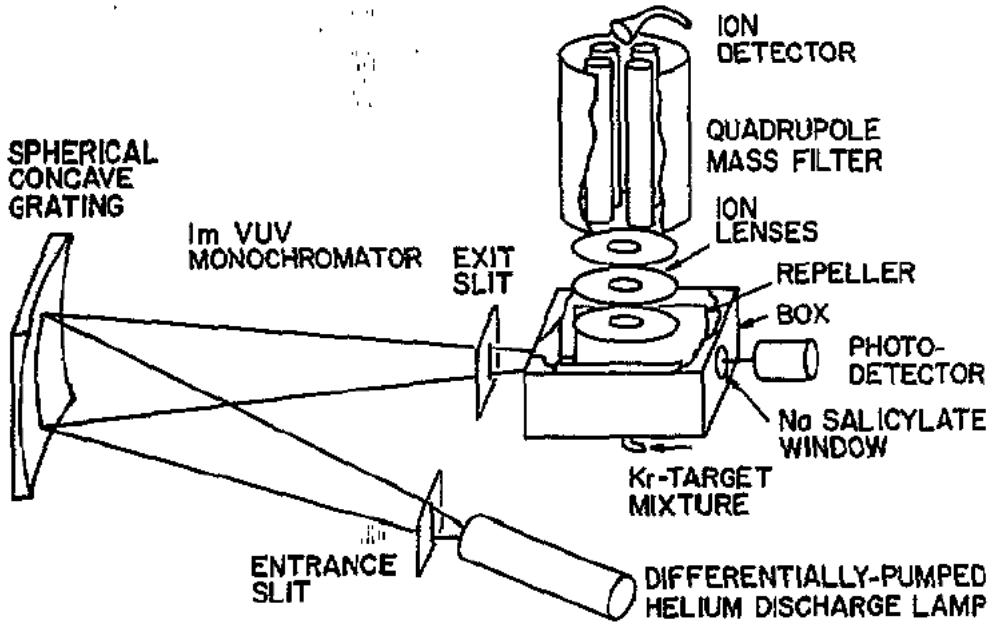

Figure 1. Schematic diagram of the VUV photoionization apparatus used for attachment studies (Chutjian and Alajajian 1985a, b).

$$Kr(^1S_0) + \hbar\omega \rightarrow Kr^+(^2P_{1/2}) + e^-(\varepsilon)$$

$$e^- + SF_6 \rightarrow SF_6^{-*}$$

$$e^- + CCl_4 \rightarrow CCl_4^{-*} \rightarrow CCl_3 + Cl^-$$

Very low collision energies

$$Kr(^1S_0) + \hbar\omega \rightarrow Kr^+(^2P_{1/2}) + e^-(\varepsilon)$$

$$e^- + SF_6 \rightarrow SF_6^{-*}$$

$$e^- + CCl_4 \rightarrow CCl_4^{-*} \rightarrow CCl_3 + Cl^-$$

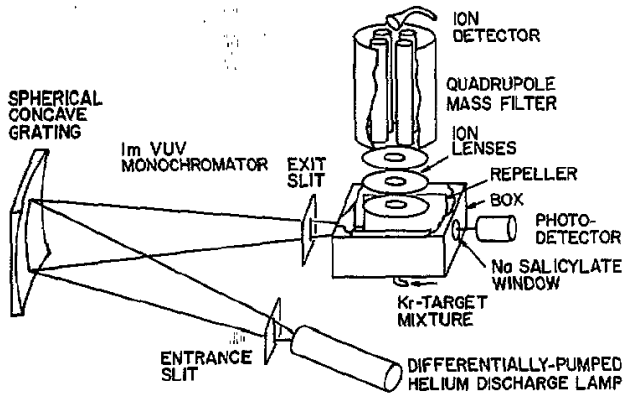

Figure 1. Schematic diagram of the VUV photoionization apparatus used for attachment studies (Chutjian and Alajajian 1985a, b).

TOPICAL REVIEW

J. Phys. B: At. Mol. Opt. Phys. **28** (1995) 1645–1672. Printed in the UK

Electron–molecule collisions at very low electron energies

F B Dunning

Department of Physics and the Rice Quantum Institute, Rice University, PO Box 1892, Houston, TX 77251, USA

10^5 Å

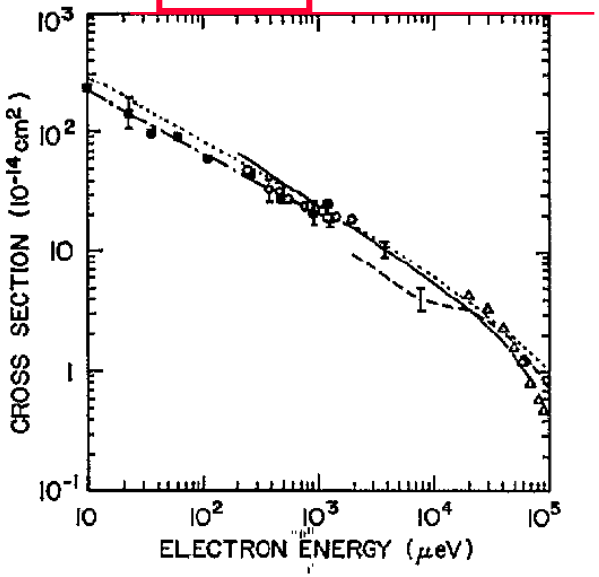

Figure 2. Cross section for electron attachment to SF_6. ■, $\bar{\sigma}_e$-K(np); — · —, $\sigma_e(v)$-K(np) (Ling *et al* 1992). ○, $\bar{\sigma}_e$-Rb(ns) (Zollars *et al* 1985); ——, free electrons (Klar *et al* 1992a, b); – – –, free electrons (Chutjian and Alajajian 1985); △, free electrons (Pai *et al* 1979, Chutjian and Alajajian 1985a); ----, theory (Klots 1976).

Electron attachment at very low electron energies

10^5 Å

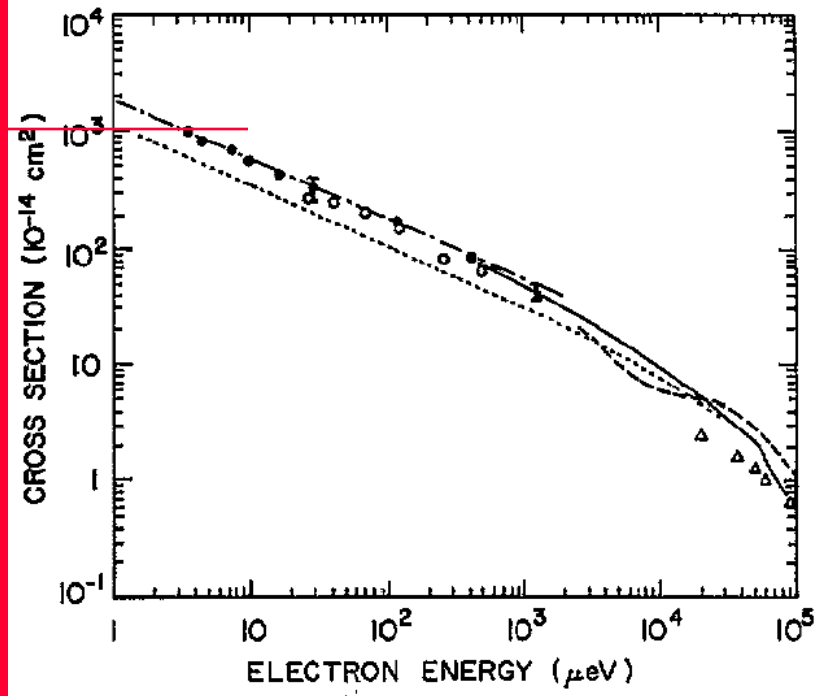

Figure 3. Cross sections for electron attachment to CCl_4. ●, $\bar{\sigma}_e$-K(np); — · —, $\sigma_e(v)$-K(np) (Frey *et al* 1994b); ○, $\bar{\sigma}_e$-K(np) (Ling *et al* 1992); ——, free electrons (Hotop 1994); – – –, free electrons (Orient *et al* 1989); △, free electrons (Christodoulides and Christophorou (1971); -----, theory (Klots 1976).

10^5 Å

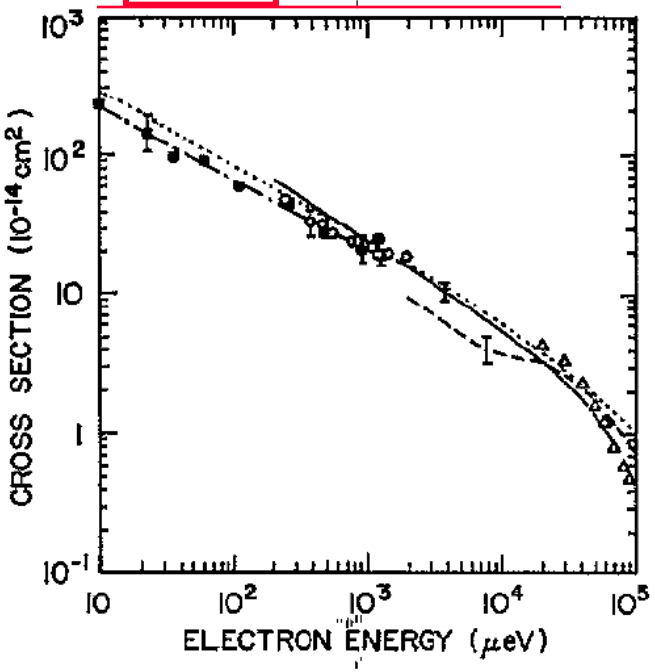

Figure 2. Cross section for electron attachment to SF_6. ■, $\bar{\sigma}_e$-K(np); — · —, $\sigma_e(v)$-K(np) (Ling *et al* 1992). ○, $\bar{\sigma}_e$-Rb(ns) (Zollars *et al* 1985); ——, free electrons (Klar *et al* 1992a, b); – – –, free electrons (Chutjian and Alajajian 1985); △, free electrons (Pai *et al* 1979, Chutjian and Alajajian 1985a); -----, theory (Klots 1976).

Molecules

2004

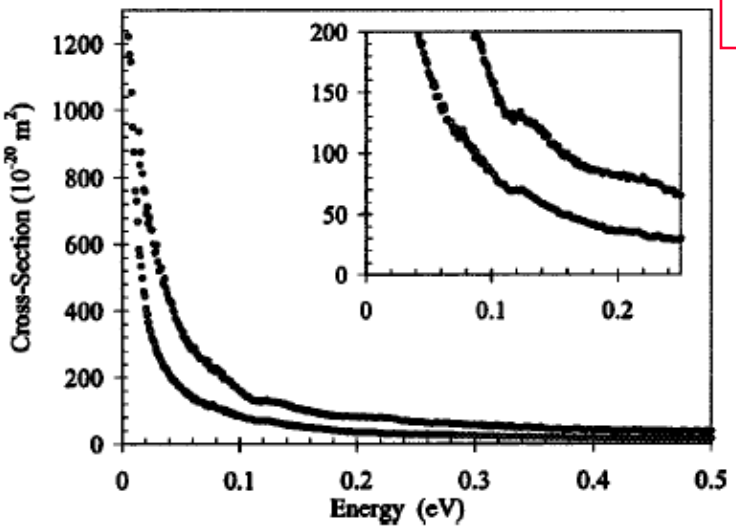

PHYSICAL REVIEW A 69, 052716 (2004)

Cold electron scattering in SF_6 and C_6F_6: Bound and virtual state channels

D. Field,[1,*] N. C. Jones,[1] and J.-P. Ziesel[2]
[1]*Department of Physics and Astronomy, University of Aarhus, DK- 8000 Aarhus C, Denmark*
[2]*Laboratoire Collisions Agrégats Réactivité (CNRS UMR5589), Université Paul Sabatier, 31062 Toulouse, France*
(Received 26 November 2003; published 20 May 2004)

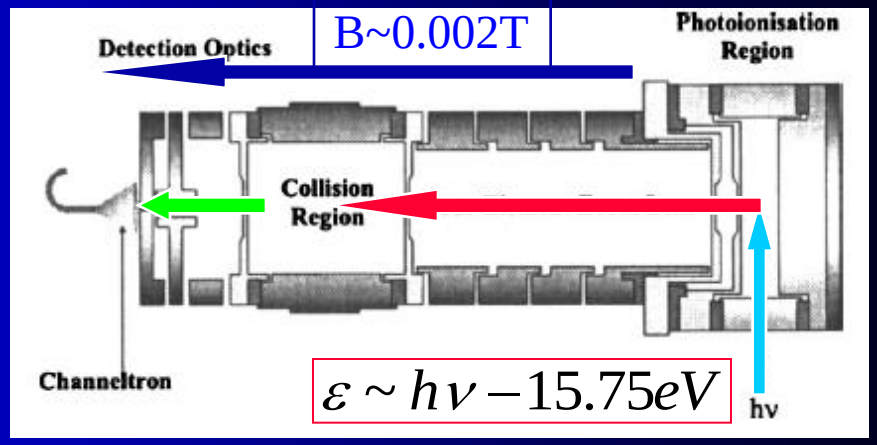

The general process which we study involves electron attachment,

$$e^- + M \rightarrow M^{-*}, \quad M = SF_6, C_6F_6, \qquad (1)$$

FIG. 1. A scale diagram of the apparatus. Monochromatic synchrotron radiation from ASTRID ($h\nu$) enters a photoionization region containing Ar. Photoelectrons, expelled by a weak electric field, are focused by a four-element lens [38] into a collision chamber containing the target gas. Transmitted electrons are detected at the channel electron multiplier (channeltron) situated beyond some further electron optics. The apparatus may be immersed in an axial magnetic field of 2×10^{-3} T.

B=0.002T

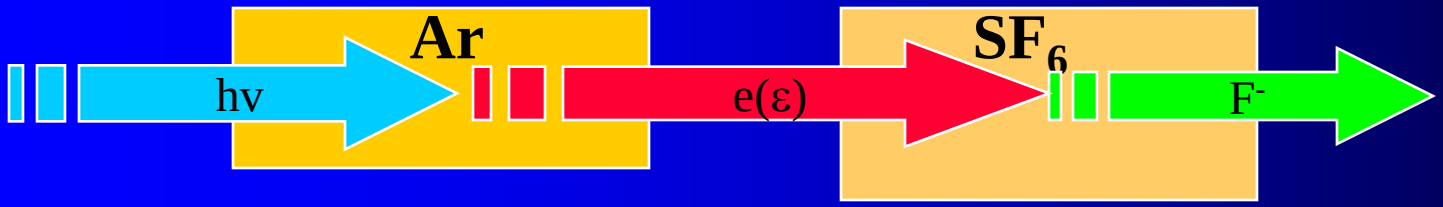

$Ar + h\nu \rightarrow Ar^+ + e(\varepsilon)$

$\varepsilon \sim h\nu - 15.75eV$

$SF_6 + e(\varepsilon) \rightarrow X^- + Y$

Molecules

2008

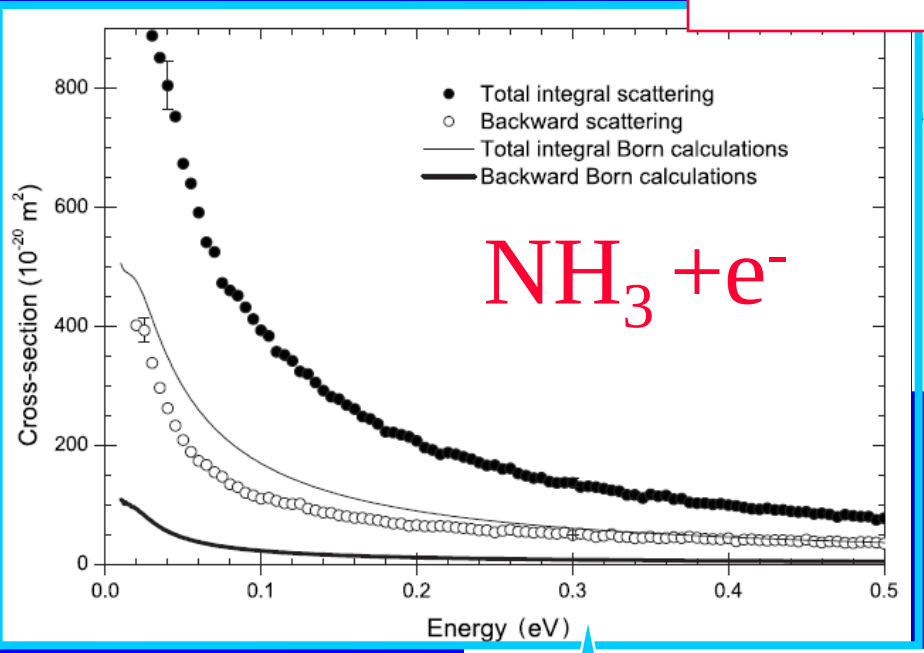

PHYSICAL REVIEW A **78**, 042714 (2008)

Scattering of cold electrons by ammonia, hydrogen sulfide, and carbonyl sulfide

N. C. Jones,[1] D. Field,[2,*] S. L. Lunt,[3] and J.-P. Ziesel[4]
[1]*Institute for Storage Ring Facilities (ISA), University of Aarhus, DK-8000 Aarhus C, Denmark*
[2]*Department of Physics and Astronomy, University of Aarhus, DK-8000 Aarhus C, Denmark*
[3]*Kittiwake Developments Ltd, Littlehampton, West Sussex BN17 7LU, United Kingdom*
Laboratoire Collisions Agrégats Réactivité (CNRS-UPS UMR5589), Université Paul Sabatier, 31062 Toulouse, France
(Received 2 July 2008; published 29 October 2008)

Experimental data obtained with a high-resolution transmission experiment are presented for the scattering of electrons in the energy range 20 meV–10 eV for NH_3, 25 meV–10 eV for H_2S, and 15 meV–2.5 eV for OCS. Data include cross sections for both integral scattering and scattering into the backward hemisphere, the latter up to 650 meV impact energy, with an electron energy resolution of between 1.6 and 3.5 meV. The new data allow the first detailed comparison with theory for the energy regime dominated by rotationally inelastic and elastic scattering for these species. It is evident that theory still lacks quantitative predictive power at low energy, although qualitative agreement is consistently good for all three species. A discussion is given of the possible presence of a virtual state in OCS scattering as recently proposed on theoretical grounds.

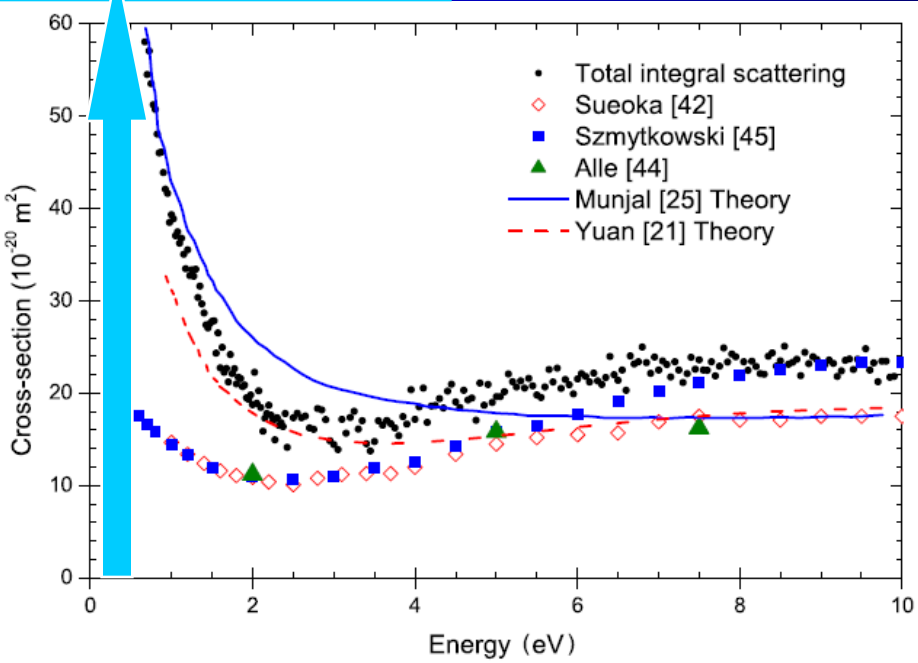

$NH_3 + e^-$

FIG. 1. (Color online) NH_3: the variation of the sum of the integral elastic and inelastic cross sections, $\sigma_{T,I}$, between 0.675 and 10 eV. Also shown are experimental data from Sueoka *et al.* [42], Szmytkowski *et al.* [45], and Alle *et al.* [44] and theoretical values from Munjal *et al.* [25] and Yuan *et al.* [21].

Molecules cross section for interaction with electrons

2008

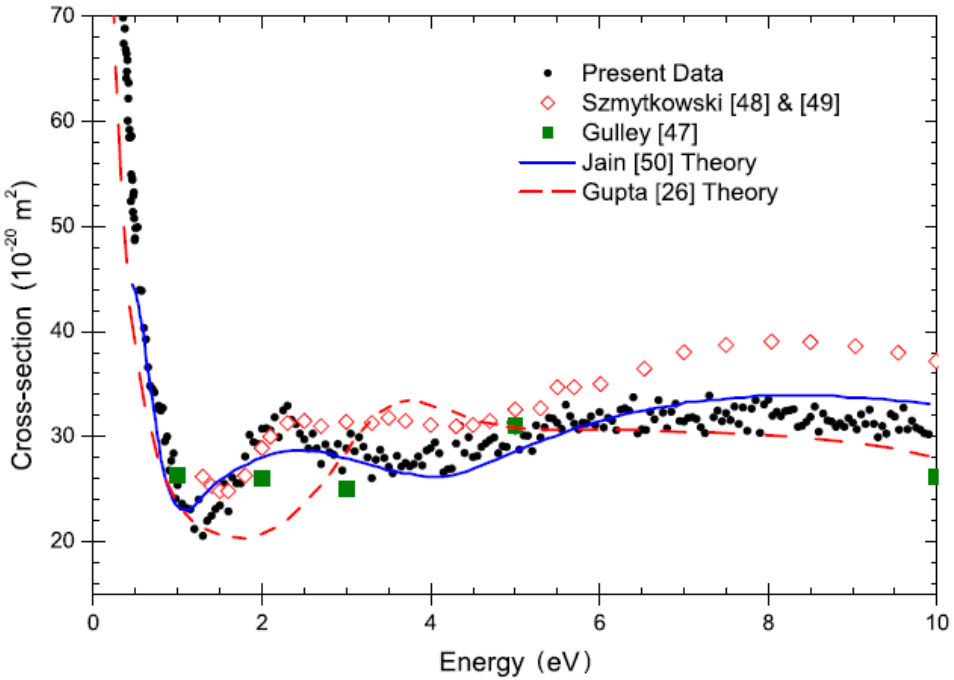

$H_2S + e^-$

FIG. 3. (Color online) H_2S: the variation of the sum of the integral elastic and inelastic cross sections, $\sigma_{T,I}$, between 380 meV and 10 eV. Also shown are experimental data in Szmytowski *et al.* [48,49] and Gulley *et al.* [47] and theoretical values from Jain *et al.* [50] and Gupta *et al.* [26].

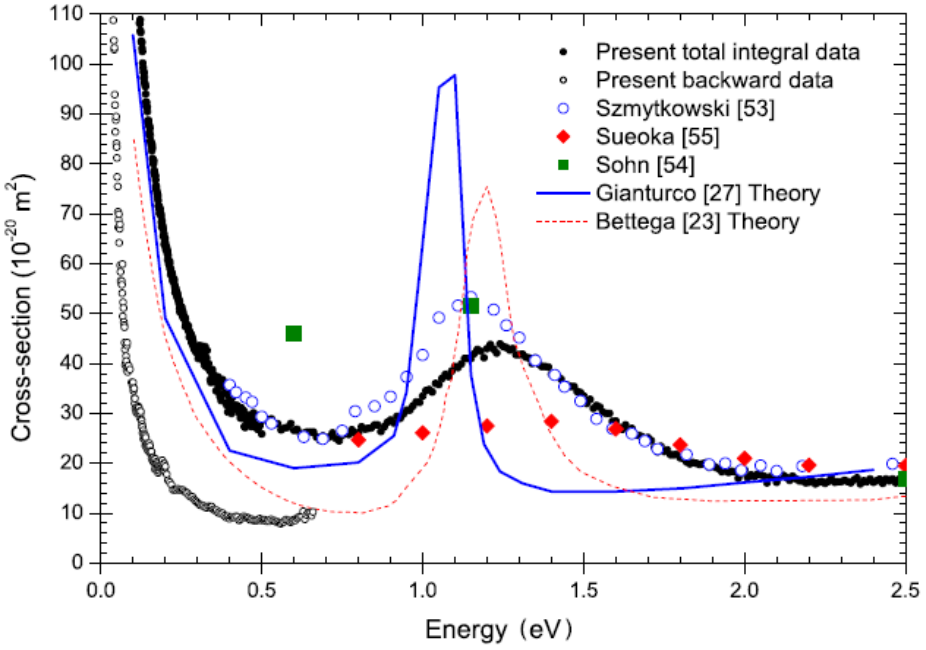

$OCS + e^-$

FIG. 5. (Color online) OCS: the variation of the sum of the integral elastic and inelastic cross sections, $\sigma_{T,I}$, between 120 meV and 2.5 eV, and the elastic and inelastic backward scattering cross section into the backward 2π sr, between 39 and 650 meV. Also shown are experimental values from Szymtkowski *et al.* [53], Sueoka *et al.* [55], and Sohn *et al.* [54] and theoretical values of integral cross sections from Gianturco *et al.* [27] and Bettega *et al.* [23].

Molecules

2006

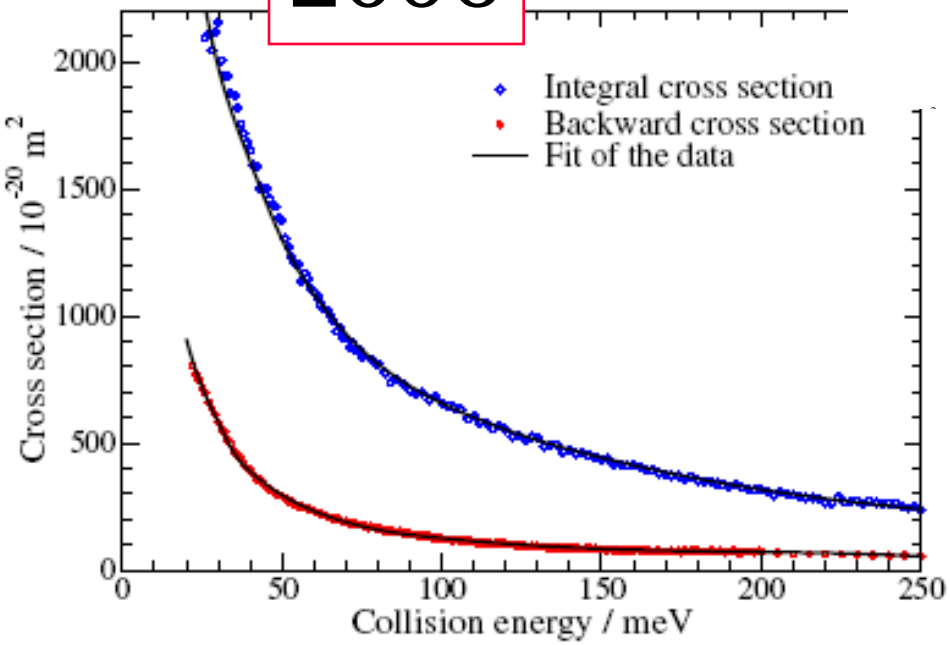

PRL 97, 123202 (2006) PHYSICAL REVIEW LETTERS week ending 22 SEPTEMBER 2006

Rotational Excitation of H_2O by Cold Electrons

R. Čurík,[1] J. P. Ziesel,[2] N. C. Jones,[3] T. A. Field,[4] and D. Field[3,*]
[1]*J. Heyrovský Institute of Physical Chemistry, Dolejškova 3, 18223 Prague 8, Czech Republic*

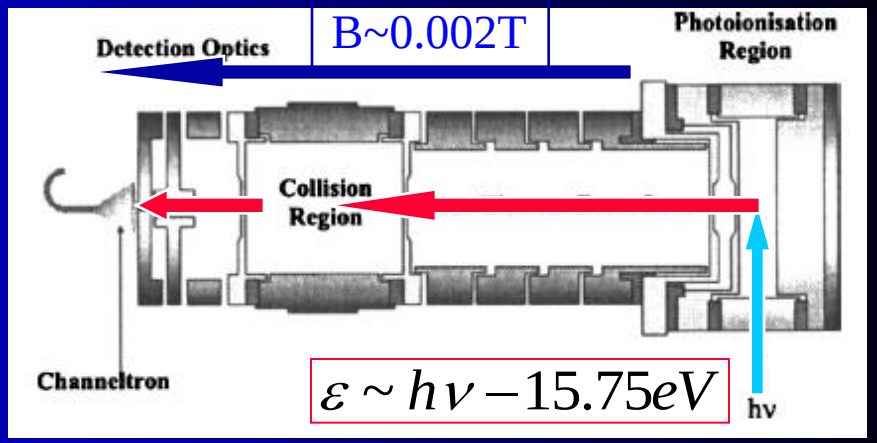

Experimental data are presented for the scattering of electrons by H_2O between 17 and 250 meV impact energy. These results are used in conjunction with a generally applicable method, based on a quantum defect theory approach to electron-polar molecule collisions, to derive the first set of data for state-to-state rotationally inelastic scattering cross sections based on experimental values.

B=2x10^{-3}T

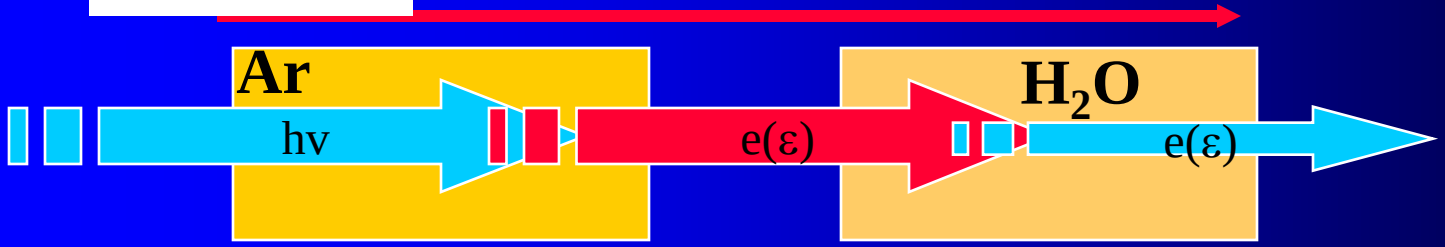

Ar +hν➔Ar$^+$+e(ε)

$\varepsilon \sim h\nu - 15.75eV$

H_2O (j_0) + e(ε_1)➔ H_2O($j>j_0$) + e(ε_2)

Molecules

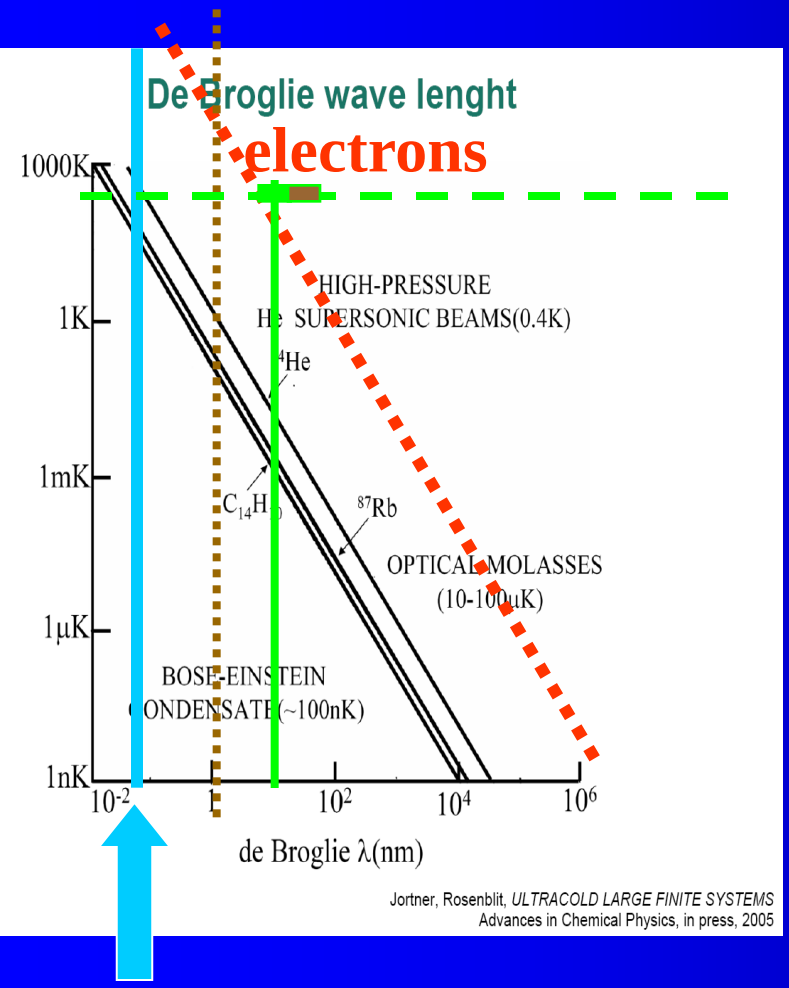

Jortner, Rosenblit, *ULTRACOLD LARGE FINITE SYSTEMS*
Advances in Chemical Physics, in press, 2005

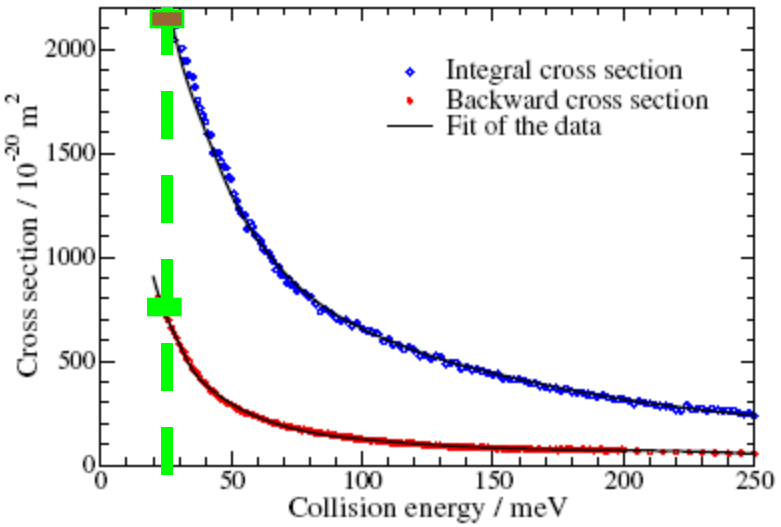

FIG. 1 (color online). Integral (upper set) and backward cross sections (lower set) for scattering of electrons by H_2O as a function of electron impact energy. Values are ±5%. The solid lines are fits to theory (see text).

$$\lambda = \frac{h}{p} = \frac{h}{mv}\sqrt{1 - \frac{v^2}{c^2}}$$

$$\sigma \sim \pi\lambda^2 \sim 1/\varepsilon$$

Molecules -rotational excitation

2006

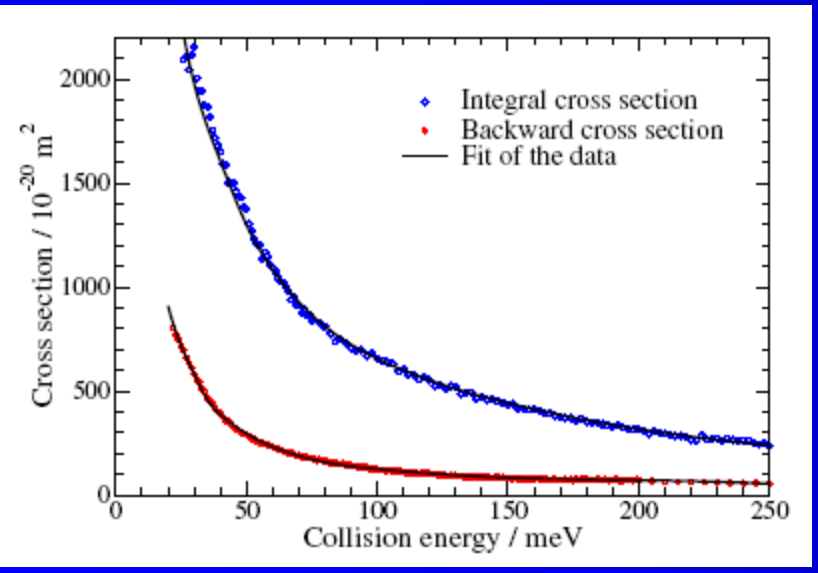

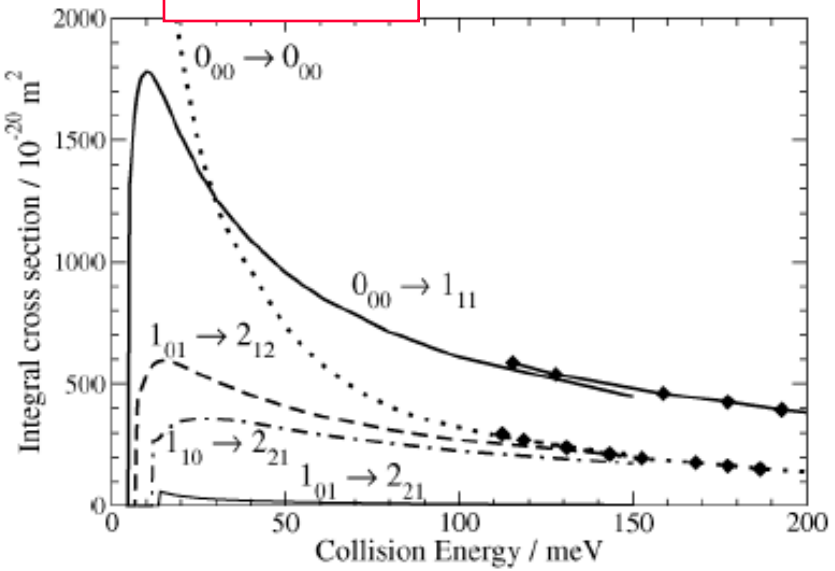

FIG. 3. Selected state-to-state integral cross sections for rotational excitation of the H_2O molecule determined from experimental data. Full curves represent results for para-H_2O and dashed for ortho-H_2O. The dotted curve represents elastic scattering for para-H_2O in its lowest rotational state. Curves with diamonds show the results of *R*-matrix calculations in Ref. [12].

$H_2O\ (j_0) + e(\varepsilon_1) \rightarrow H_2O(j>j_0) + e(\varepsilon_2)$